

Multifaceted functions of Rab23 on primary cilium and Hedgehog signaling-mediated granule cell proliferation

CHH Hor^{*1,2}, WY Leong², and ELK Goh^{*2,3,4,5}

Affiliations:

¹Department of Chemistry, Research Cluster on Health and Drug Discovery, Faculty of Science, Hong Kong Baptist University, Kowloon Tong, Hong Kong SAR

²Neuroscience Academic Clinical Programme, Duke-NUS Medical School, Singapore

³Department of Research, National Neuroscience Institute, Singapore

⁴Neuroscience and Mental Health Faculty, Lee Kong Chian School of Medicine, Nanyang Technological University, Singapore

⁵KK Research Center, KK Women's and Children's Hospital, Singapore

*Co-corresponding authors

Email: Eyleen_Goh@nni.com.sg; catherinehor@hkbu.edu.hk

Running title: Rab23 in hedgehog signaling and cerebellar development

Key words: Ciliary signaling, Sonic hedgehog, Primary cilium, Rab GTPase, Ciliogenesis, Medulloblastoma

Number of Figures: 6

Conflict of Interest

The authors declare no conflict of interest.

Abstract

Sonic Hedgehog (Shh) signaling from the primary cilium drives cerebellar granule cell precursor (GCP) proliferation. Mutations of hedgehog (Hh) pathway repressors could cause medulloblastoma, the most prevalent and malignant childhood brain tumor that arises from aberrant GCP proliferation. We demonstrate that brain-specific knockout of a Shh pathway repressor *Rab23* in mice caused mis-patterning of cerebellar folia and elevated GCP proliferation during early development, but with no prevalent occurrence of medulloblastoma at adult stage. Strikingly, *Rab23*-depleted GCPs exhibited up-regulated basal level of Shh pathway activities despite reduced ciliation, and were desensitized against stimulations by Shh and Smoothed (Smo) agonist in primary GCP culture. These results illustrate dual functions of *Rab23* in repressing the basal level of Shh signaling, while facilitating Shh signal transduction via Shh/Smo on primary cilium. Collectively, our findings unravel instrumental roles of *Rab23* in GCP proliferation and ciliogenesis. *Rab23*'s potentiation of Shh signaling pathway through the primary cilium and Smo, suggests a potential new therapeutic for Smo/primary cilium-driven medulloblastoma.

Author Summary

C.H.H conceived, designed, lead, and performed all *in vitro* and *in vivo* experiments, analyzed data and wrote the manuscript. W.Y performed QPCR experiments and primary GCP cultures and analyzed data. E.L.G conceived and directed the study.

1 **Introduction**

2

3 Cerebellar development in mammals is highly dependent on Shh signaling. In
4 particular, Shh signaling dictates the proliferation of granule cell precursors (GCP)
5 (1,2). GCPs give rise to granule neurons, the most abundant neuronal type in the brain.
6 In the developing cerebellum, GCPs receive mitotic signals from Shh ligands released
7 from the neighboring Purkinje cells to sustain its proliferation (1,2). Besides paracrine
8 Shh signaling, GCPs were also capable of self-regulated autocrine-induced cell
9 proliferation (3). Perturbation of Shh pathway activity during early embryonic or
10 postnatal development results in cerebellar dysplasia, hypoplasia as well as malignant
11 childhood brain tumor medulloblastoma (2,4–7). For example, genetic mutations of
12 Shh signaling components such as *Patched (PTCH)*, *Smoothed (SMO)*, *Gpr161* or
13 *Suppressor of Fused (SUFU)* are known to lead to the formation of medulloblastoma
14 (8–11)(12).

15

16 In the past decade, emergence of primary cilium as an indispensable organelle for Shh
17 signal transduction has facilitated discoveries that recognized the seminal roles of
18 primary cilium in cerebellar development and medulloblastoma formation. The primary
19 cilium is a non-motile cilium found on the surface of nearly every cell. It functions
20 primarily as an “antenna” on the cell membrane to receive and transduce extracellular
21 signals. In the Shh pathway, Shh ligand binds to the Ptch receptor to release its
22 suppression of Smo on the cell membrane. This subsequently triggers Smo and
23 cytosolic factors such as the Gli transcription factors and SuFu to interact within the
24 primary cilium before translocating into the nucleus to activate Shh downstream target
25 genes (13–15). Although the exact molecular mechanism and trafficking cargoes that

26 mediate dynamic ciliary entry and exit of Shh signaling components remain
27 incompletely understood, it has been well established that Shh signal transduction is
28 inevitably deregulated in the absence of a functional primary cilium. For instance,
29 knockout (KO) of genes known to be required for primary cilium formation (i.e. *Kif3a*
30 or *Ift88*) diminished Shh activities in the cerebellum and contributed to the
31 manifestation of cerebellar hypoplasia and distorted foliation due to substantial
32 shrinkage of granule cell precursors pool (16,17).

33

34 Intriguingly, recent findings have revealed that the primary cilium could exert both
35 inducing or suppressing forces on Shh pathway and cancer progression (15,18,19).
36 Depending on the pathogenic origin of the medulloblastoma, primary cilia could
37 potentiate tumor growth driven by Smo, and on the other hand, inhibit tumor growth
38 driven by Gli2 (18). Adding to the complexity of the tumor biology, the same study
39 also showed that there are ciliated and non-ciliated sub-categories of medulloblastoma,
40 with the ones bearing primary cilia often associated with increased Shh and Wnt
41 pathway activities, whereas those without cilia do not exhibit Shh or Wnt pathway
42 activation (18). Given the opposing functions of primary cilium on Shh pathway-
43 mediated tumor progression, as well as the heterogeneity in ciliation capacity among
44 the tumor cells; the multifaceted functions of primary cilium might underlies variable
45 patients' responses to Smo-specific drug, Vismodegib treatment in the clinical trials
46 that targets Shh-subtype medulloblastoma (20,21,22). Therefore, further insights on the
47 interaction between primary cilium and the Shh pathway, and their roles in GCP
48 proliferation would lay critical foundation for further development of effective
49 intervention for medulloblastoma.

50

51 Rab23 is a brain-enriched small GTPase (21) known to antagonize the Shh pathway *in*
52 *vivo*, as evidenced by developmental mouse genetic studies. In humans, mutations of
53 *RAB23* cause Carpenter syndrome, an autosomal recessive disorder characterized by
54 aberrant skull fusion, polydactyly and branchyductyly. Other variable developmental
55 abnormalities including heart defect, genu valgum, cornea defect, umbilical hernia,
56 obesity, developmental delay, as well as central nervous system (CNS)-related
57 conditions including cerebral and cerebellar malformations, hydrocephaly, intellectual
58 disability and schizophrenia (22–29). In mouse, the *Rab23*-encoding *open brain (opb)*
59 null allele mutant exhibited embryonic lethality at mid-gestation stage, exencephaly
60 and ectopic neural tube ventralization (30,31), which largely recapitulated the
61 phenotypes of other Shh repressor mutants such as *Patched1 (Ptch1)* and *Suppressor*
62 *of fused (Sufu)* KOs (32–34). Nonetheless, owing to the early embryonic lethality of
63 *Rab23*-null mutant in mouse, true implications of Rab23 in Shh signaling-mediated
64 CNS development beyond the mid-gestation stage are not known.

65

66 Genetic study revealed that *Rab23* represses Hh activities via *Gli2* and promotes the
67 proteolytic cleavage of *Gli3* into its cleaved repressor form (31). In addition, *Rab23*
68 also appeared to regulate Hh pathway activity through *Smo*. Concomittant deletion of
69 *Smo* in the *Rab23*-null mutant has partially weakened Shh activation level in the neural
70 tube as compared to that of *Rab23* mutant (31). Besides, a molecular study in
71 mammalian cell line model reported that Rab23 mediates the protein turnover dynamics
72 of *Smo* in the primary cilium, although it was not clear as to how this may influence
73 Shh pathway activity(35). Another *in vitro* study further revealed that Rab23
74 antagonizes the nuclear translocation of *Gli1* transcription activator to impede Shh
75 pathway activation (36). Taken together, these findings suggest that Rab23 casts

76 multiple actions in the modulation of Hh signaling cascade. However, how it
77 orchestrates Shh pathway in the context of GCP proliferation and medulloblastoma
78 formation remains to be determined.

79

80 Although independent studies have implicated the functions of *Rab23* in primary cilium
81 formation and ciliary trafficking, its role in ciliogenesis remains obscure due to
82 inconsistent observations from different cell types. For instance, overexpression of the
83 dominant-negative form, Rab23DN perturbed ciliation in the immortalized retinal
84 pigmented epithelial cells (37). Supporting this observation, a recent study has
85 identified that the GDP-GTP exchange factors (GEF) of Rab23 namely Inturned and
86 Fuzzy, were localized to the primary cilium at proximal end, and played essential role
87 in the primary cilia formation of human and mouse cells(38). The same study
88 demonstrated that depletion of GEF (i.e. Intu and Fuzz), or Rab23 perturbed primary
89 cilium formation in culture IMCD3 cells. On the contrary, *Rab23*^{-/-} mouse embryo
90 showed unaltered node cilia during early development(39). Taken together, these data
91 suggest that Rab23's action in the primary cilium formation is possibly operating in a
92 context-dependent manner. In the IMCD3 cells that have morphologically normal
93 primary cilium, Rab23 forms protein complex with Kif17 and Dopamine receptor 1
94 (D1R), and it was required for their ciliary localization (40,41). These findings
95 indicated that Rab23 plays crucial roles in ciliary protein targeting. Despite the known
96 function of Rab23 in primary cilium formation and Hh signaling, as well as the long
97 perceived function of primary cilium-dependent Hh signaling in GCP proliferation,
98 whether Rab23 is required for the primary cilium formation in the CNS and cerebellar
99 GCP is not known. Moreover, how Rab23 may mediate primary cilium-dependent Shh

100 signal transduction, and its impact on GCP proliferation and cerebellar development
101 remain to be further characterized.

102

103 In this study, we demonstrate that conditional KO of *Rab23* in the developing mouse
104 brain at E10.5 resulted in abnormal cerebellar foliation, as well as unexpected opposing
105 changes in the cerebellar sizes and Shh activities during embryonic and postnatal
106 cerebellar development. Interestingly, our data suggest that loss of *Rab23* did not casue
107 medulloblastoma despite an increase in the basal level of Shh pathway activities and
108 GCP proliferation. We found that KO of *Rab23* affected ciliation in GCP, and rendered
109 the cells less responsive to pathway activation by Shh and Smo agonist. These results
110 suggest that the *Rab23*-KO GCPs have an attenuated response to paracrine Shh stimuli
111 from primary cilium. Taken together, we have uncovered novel functions of *Rab23* in
112 GCP proliferation, acting both positively and negatively via Shh signaling. Our results
113 indicate that *Rab23* represses basal level of Shh signaling pathway activities, while
114 facilitates Smo-mediated Shh pathway activation in a primary cilium-dependent
115 manner.

116

117

118 **Results**

119

120 ***Rab23* dictates proper cerebellar morphogenesis and development**

121 In order to investigate the functions of *Rab23* in central nervous system (CNS)
122 development, mouse bearing Nestin-cre (*Nes*) was crossed with *Rab23-floxed* (42)
123 homozygous mutant to achieve conditional knock-out (CKO) of *Rab23* in the neural
124 progenitor cells at approximately embryonic (E) day 10.5. Gross morphological

125 examination of the whole brain isolated from Nes-CKO mutant revealed noticeable
126 cerebellar enlargement at earlier developmental stages (i.e. postnatal (P) day one and
127 four) but appeared smaller at later adult stage as compared to the control (*Rab23^{ff/ff}*)
128 counterpart (Fig. 1A-B, E, yellow asterisk). Histological examination of the mid-sagittal
129 cerebellar sections by hematoxylin-eosin (H&E) staining revealed cerebellar dysplasia
130 in Nes-CKO brains. This was consistently observed at P1, P4 and adult stages (Fig. 1C-
131 D, F). Disrupted patterning of the cerebellar folia was more prominent at the caudal
132 region. Moreover, the external granular layer (EGL) at the posterior lobules appeared
133 thicker and disorganized as compared to the control group (Fig. 1C-D, red arrows). In
134 the adult mutant, the posterior cerebellar folia were irregularly formed and lack
135 distinctive laminar layering of molecular layer (ML), Purkinje cell layer (PCL) and
136 internal granule layer (IGL) (Fig 1F). Taken together, these data indicate that a loss of
137 *Rab23* resulted in defects in cerebellar folia patterning during postnatal CNS
138 development.

139

140 **Depletion of Rab23 disrupted cerebellar radial glial scaffold and innervations of** 141 **granule cells**

142 The disorganized laminar layering, as well as the cerebellar folia anomaly prompted
143 further examination of the Bergmann glial (Bg) scaffold, which acts as the
144 cytoarchitectural scaffold to aid in neuronal migration and lamination (43–45). We used
145 antibodies against Nestin and glial fibrillary acidic protein (GFAP) to immunolabel
146 radial glia and the Bg scaffold at early postnatal and later adult stages respectively. In
147 the *Rab23^{ff/ff}* (control) group, radial fibers of Bg at P1, P4 and P15 appeared
148 perpendicularly aligned and extended from the cell bodies at the lower ML and PCL
149 towards the pial surface of the cerebellum. In contrast, the processes of Nes-CKO

150 mutant Bg in the disrupted lobules appeared tangled and misaligned, with some of them
151 unable to extend processes to the pial surface, thus indicating an impairment of the Bg
152 scaffold (Fig. 2A-C). Additionally, hyperplastic lesion-like ectopic nuclei accumulation
153 were detectable at the pial surface in P4 (Fig 2B, asterisk) and adult cerebellum (Fig.
154 2D, white arrows). In line with this defect, the NeuN-positive granule cells in the adult
155 mutant were aberrantly localized to the pial surface and the ML instead of the deeper
156 IGL. In addition, a subpopulation of the granule cells was randomly scattered at the
157 posterior region, concomitant with a loss of laminar structure. The cell soma of GFAP-
158 positive astrocytes/Bg were also found to be ectopically misplaced at the pial surface
159 and ML, indicating a misalignment of radial glial scaffold at the adult stage (Fig. 2D,
160 D', D''). These data indicate that an abnormal glial scaffold in Nes-CKO mutants may
161 hinder proper invagination and migration of granule cells to the deeper IGL during early
162 postnatal cerebellar development.

163

164 Given the defective radial glial scaffold and ectopic accumulation of granule cells at
165 the pial surface and ML, we asked if the inward radial migration of granule cell at the
166 earlier embryonic and postnatal stages was affected. Anti-Pax6 antibody was used to
167 immunolabel both amplifying granule cell precursors (GCP) transiently residing in the
168 EGL (source of granule cells), and the early inwardly migrated post-mitotic granule
169 cells in the granular layer at E15.5 (46). The Pax6-expressing granule cells in the
170 control group were more well-dispersed and scattered further into the deeper granule
171 layer. Conversely, *Rab23*-depleted granule cells appeared less dispersed and are largely
172 confined to the region adjacent to the EGL (Fig. 3A, yellow dotted lines). Because all
173 granule cells arise from the EGL and innervate the inner granular layer as they undergo
174 maturation, we quantified the innervation/migration rate by counting the number of

175 Pax6-positive cells that have populated the inner granular layer (innervated) against
176 total Pax6-positive cells. Indeed, the proportion of innervated granule cells in the Nes-
177 CKO mutant appeared markedly reduced compared to the control counterpart (Fig. 3B),
178 suggesting an impaired or delayed innervation. In addition, a two-hour EdU-pulse
179 labeling assay was used to track all early innervated progenitor cells. The proportion of
180 EdU-labelled cells that have innervated (from EGL – magenta arrows, and VZ – yellow
181 arrows) the granular layer was scored against all EdU-labelled cells. Similarly, *Rab23*-
182 depleted cells showed a lower percentage of innervated cells in the granular layer (Fig.
183 3C).

184

185 For the postnatal stage, we examined the migration of granule cells by 48 hours EdU-
186 pulse labelling for P5 to P7. The percentages of cell innervation in different lobules
187 were then analyzed by quantifying the percentages of EdU-labelled cells residing in the
188 EGL, ML and IGL of each lobule. In agreement with the results from the embryonic
189 stage (Fig. 3A-C), the proportions of mutant cells reaching IGL were greatly reduced,
190 concomitant with an increase in the percentage of cells that are accumulated in the EGL
191 (Fig. 3D-E). Taken together, these data suggest that deletion of *Rab23* caused a
192 misalignment of the radial glial scaffold, leading to perturbations in granule cells
193 innervation and lamination. As a result, the cerebellar laminae and folia could not be
194 properly formed during postnatal cerebellar development.

195

196 **Rab23-ablation caused thickened EGL and enhanced GCP proliferation, but no**
197 **discernible tumorigenesis**

198 In view of the thickened EGL observed in H&E staining, as well as the enlarged
199 cerebellum of Nes-CKO at P1 and P4, a more detailed analysis of cell proliferation is

200 warranted. We performed co-immunolabeling of Pax6 and Calbindin to visualized GCP
201 and Purkinje cells respectively. At P1, there was an overall increase in the number of
202 Pax6-expressing GCPs in the Nes-CKO mutant compared to the control. Besides, the
203 Pax6-labelled EGL in Nes-CKO appeared greatly thickened, more so near the posterior
204 folia (Fig. 4A, white asterisks). On the other hand, the Calbindin-expressing Purkinje
205 cells in the mutant PCL appeared to be lower in density and more sparsely distributed
206 as compared to the more densely aligned Purkinje cell layer in the control counterpart
207 (Fig. 4B), implying a perturbed PCL lamination.

208

209 Two hours EdU-pulse labelling was performed on E15.5 and P4 animals to probe GCP
210 proliferation in further details. Compared to the control, the pools of EdU-positive
211 proliferative cells are substantially expanded in the EGL of Nes-CKO mutant at both
212 time points (Fig. 4C-D, red and yellow double heads arrows), indicating aberrantly
213 enhanced GCP proliferation during both embryonic and postnatal cerebellar
214 development. These phenotypes were further confirmed by a quantification of EdU-
215 positive nuclei in the EGL at E15.5, which revealed a significant up-regulation of
216 proliferative cells in the mutant EGL as compared to the control group (Fig. 4E).
217 Accordingly, another cell proliferation marker, *Ki67*, and a GCP-specific marker *Atoh1*,
218 also showed markedly elevated expression levels in the cerebellar tissue of Nes-CKO
219 mutants (Fig. 4F). Taken together, these data suggest that depletion of *Rab23*
220 potentiated GCP proliferation during early cerebellar development. Excessive GCP
221 proliferation often give rise to medulloblastoma (47)(48,49). Given this, one would
222 expect the development of medulloblastoma at a later postnatal stage. However, we did
223 not find detectable manifestation of medulloblastoma in adult mutant animals, despite

224 the occurrence of hyperplastic lesions-like tissue clumps at P4 (Fig. 1F, 2B-asterisk,
225 D-white arrows).

226

227 **Shh signaling is differentially perturbed in the developing cerebellum**

228 Previous genetic studies have reported that *Rab23* negatively regulates Shh signaling
229 (30,50). As Shh signaling is the key signaling pathway that modulates GCP
230 proliferation (1,2,51,52), we reasoned that it is likely a main factor driving aberrant
231 GCP proliferation in the *Rab23*-deficient cerebellum. To address this possibility, we
232 examined the expressions of *Gli* transcription factors, which are downstream effectors
233 of Shh signaling in CNS development. The Shh signaling activities in cerebellar tissue
234 were examined in both embryonic E15.5 and late postnatal P15. In accordance with the
235 increased CGP proliferation in Nes-CKO at E15.5 and P4, Shh signaling pathway
236 activities were robustly up-regulated at E15.5, as shown by an increase in *Gli1* and *Gli2*
237 expressions compared to the control group (Fig. 5A). Intriguingly, at P15, the
238 expression level of *Gli1* transcripts was significantly down-regulated in the Nes-CKO
239 mutant cerebellum, despite up-regulated levels of *Gli2*, *Gli3*, *Ki67* and *Atoh1* (Fig. 5B).
240 Because *Gli1* activates Shh-regulated genes, and its expression is dependent on both
241 *Gli2* and *Gli3*, it could serve as the ultimate readout of Shh signaling pathway activity
242 (C Brian Bai & Joyner, 2001; C Brian Bai, Stephen, & Joyner, 2004; Lee, Platt,
243 Censullo, & Ruiz i Altaba, 1997). We also compared the expression profile of *Gli1*
244 transcripts at embryonic and postnatal stages. Compared to the control group which
245 exhibited relatively unaltered *Gli1* transcript level between E15.5 and P15, the Nes-
246 CKO mutant showed a significant reduction in *Gli1* transcript level at P15 compared to
247 its embryonic stage (Fig. 5C). Given the perturbed Shh signaling pathway activities, we
248 further examined if the *Shh* transcripts were affected. Interestingly, *Shh* transcripts level

249 in the Nes-CKO appeared largely unchanged at both developmental time points (Fig.
250 5A-B), implying that the mutant cerebellar tissues are not short of Shh stimulants
251 despite the greatly mis-patterned cerebellum. Taken together, these data show that the
252 Shh signaling activities in the Nes-CKO mutants were initially enhanced during
253 embryonic cerebellar patterning, but became down-regulated at later postnatal time
254 point as compared to the control counterpart. Notably, this correlated well with the
255 differential changes in the cerebellar size as aforementioned (Fig. 1A-B, E). Together,
256 these results revealed that Shh signaling pathway activities were differentially
257 perturbed as a result of Rab23 deficiency during embryonic and postnatal stages of
258 cerebellar patterning.

259

260 **Rab23 could regulate Shh signaling in the GCP at basal level as well as in a cilium-**
261 **dependent manner**

262 The alterations of Shh signaling pathway activities on GCP in the whole cerebellar
263 tissues could be a secondary effect resulting from abnormal changes in the
264 cellular/tissue composition. We ruled out this possibility by monitoring Shh signaling
265 in primary GCP culture isolated from P7 cerebellar tissue. Primary culture data show
266 that *Rab23*-KO GCP indeed exhibited elevated expressions of *Gli1* mRNA at the basal
267 level, indicating an over-activation of Shh pathways in the Nes-Cre mutant GCP.
268 Accordingly, primary culture of mutant GCP also displayed potentiated cell
269 proliferation, as illustrated by the up-regulation of *Atoh1* and *Ki67*, as well as an
270 increase in the percentage of EdU-positive proliferative cells (Fig. 6A-C). Furthermore,
271 Shh pathway over-activation and cell proliferation were significantly inhibited by co-
272 expressing *Rab23* wild-type cDNA, or its constitutive active form, *Rab23^{QL}*, in the KO
273 GCP (Fig. 6A-C), suggesting that the effects observed were indeed due to the loss-of

274 *Rab23* gene functions. Together, these results suggest a negative role for *Rab23* in
275 regulating Shh signaling-mediated GCP proliferation.

276

277 Previous findings have demonstrated that primary cilium is required for Shh signaling-
278 mediated CGP proliferation during cerebellar development (16,17). *Rab23* has also
279 been reported to be involved in ciliogenesis and ciliary signaling in other cell types
280 (40,41,56). Therefore, it is conceivable that the impact of *Rab23* on GCP proliferation
281 was exerted through changes to the primary cilia. We examined primary cilia
282 morphology in the E15.5 and P15 cerebellar GCP by immunolabeling of Arl13b, a
283 primary cilium-specific marker. Interestingly, Arl13b immunostaining showed that the
284 *Rab23*-depleted GCPs exhibited a significantly reduced number of cells bearing
285 primary cilium, whereas nearly all GCPs in the control counterpart showed positive
286 staining of Arl13b (Fig. 6E). This finding is further strengthened by the analysis of
287 primary cilia in primary GCP culture isolated from P7 cerebellar tissues, whereby the
288 *Rab23*-deleted GCPs in culture similarly displayed a significant reduction of ciliation,
289 which could be reversed by co-expressing *Rab23* wild-type cDNA, or the constitutive
290 active *Rab23QL* (Fig 6D). Taken together, our data provide the first indication that
291 *Rab23* influences ciliogenesis in the cerebellar GCP *in vivo*. Importantly, these results
292 also hinted at a novel cilium-dependent role of *Rab23* in coordinating Shh pathway and
293 GCP proliferation.

294

295 Given the perturbations in primary cilia morphology, we hypothesized that *Rab23*-KO
296 GCP may be compromised in primary cilium-dependent Shh signal transduction. In
297 order to address this hypothesis, primary GCP cultures were subjected to Shh ligand
298 stimulation *in vitro*. Despite its higher basal level of Shh signaling activities as

299 compared to control (Fig. 6A), *Rab23*-KO GCP showed markedly weaker response to
300 Shh ligand stimulation, as illustrated by a lower fold-increase in the expression of *Gli1*
301 mRNA as compared to the control counterpart (Fig. 6F). *Rab23*-KO GCPs also
302 exhibited lower fold-enhancement in cell division as compared to the control group, in
303 which the expression of *Ki67*, as well as *Atoh1* were both significantly lower than
304 control group upon Shh ligand stimulation (Fig. 6F). To check if the Shh signaling
305 occurs through Smo, GCP cultures were treated with a Smo agonist that promotes its
306 localization to the cilium. Control GCPs exhibited robust elevation *Gli1* expression 24
307 hours after SAG treatment (Fig. 6G). Conversely, *Rab23*-KO GCPs' response to SAG
308 induction was significantly compromised, as shown by lower expression level of *Gli1*
309 (Fig. 6G), thus implying a desensitization to Shh signaling at the level of primary cilium
310 and Smo. Together, these data demonstrated that silencing *Rab23* impaired ciliation
311 and GCP's response to Shh or Smo stimulations, thereby impeding Shh-mediated GCP
312 proliferation. These suggest a novel positive role of *Rab23* in modulating primary
313 cilium-dependent Shh signaling and GCP expansion during early cerebellar
314 development.

315

316 **Discussion**

317

318 Fine tuning Shh signaling during cerebellar development is essential to facilitate a
319 temporally and spatially-defined transit amplification of granule cell precursors (GCP)
320 to ensure proper patterning and growth of the cerebellar folia (2,57–59). We have
321 demonstrated here that *Rab23* has a role in the patterning and growth of cerebellar folia
322 during early cerebellar development. Deletion of *Rab23* resulted in foliation anomalies
323 due to dramatically perturbed radial glial scaffold formation, granule cells lamination

324 and GCP proliferation. This study presents *Rab23* as a novel regulator of GCP
325 proliferation, remarkably, acting both positively and negatively via the Shh signaling
326 pathway. Excitingly, our data showed for the first time that *Rab23* has a role in primary
327 cilium-dependent Shh signal transduction during cerebellar development. This
328 demonstration is made possible as the brain-specific KO of *Rab23* in our genetic model
329 did not result in mid-gestation lethality in mice as compared to a global loss of *Rab23*
330 in the *open brain* mutant.

331

332 Previous examination of primary cilia in the node of 2 to 6 somite stage *Rab23*-null
333 embryo reported largely unaltered morphology and similar overall percentage of
334 ciliation as compared to the control (39). Interestingly, unlike the node cilia, our data
335 revealed defective ciliation in the *Rab23*-null GCP during embryonic and early
336 postnatal cerebellar development. siRNA-mediated knockdown studies performed on
337 different cell lines have reported inconsistent conclusions with regards to the role of
338 *Rab23* in ciliogenesis (40,41,56,60). These discrepancies suggest that the functions of
339 *Rab23* in primary cilia could vary in a context or cell-type specific manner. Our data
340 supported a GCP-specific role of *Rab23* in ciliogenesis *in vivo*. In line with the *in vivo*
341 data, primary culture of *Rab23*-KO GCPs also showed deficiencies in ciliation and
342 compromised response to Shh ligand and SAG-mediated Smo activation, implicating a
343 disrupted primary cilium-dependent Shh signaling.

344

345 Mutations of Shh pathway repressor genes, including *Ptch1*, *Gpr161* and *Sufu*,
346 commonly lead to the development of medulloblastoma(9,10,61,62) via *Gli1*
347 upregulation (63). We showed that loss of *Rab23*, unlike other Shh repressors, did not
348 promote the development of medulloblastoma despite the basal level up-regulation of

349 *Gli1* expression in the GCPs. We further showed that the overall amount of Shh ligands
350 in *Rab23*-deleted cerebellar tissues remained relatively similar to that of control at both
351 embryonic and postnatal stages, suggesting a sufficient source of Shh stimulants in the
352 KO cerebellar tissue environment. Given the above, we deduce that one possible
353 explanation for an absence of tumorigenicity is the defective primary cilium in *Rab23*-
354 KO GCPs. The compromised response to primary cilium-dependent Shh activation may
355 lead to insufficient paracrine pathway stimulations to drive tumor formation in the
356 *Rab23*-KO cerebellum. This is in line with the indispensable role of primary cilium for
357 medulloblastoma formation (18,64).

358

359 Harboring the primary cilium defect in GCP, *Rab23*-KO cerebellum partially
360 phenocopied other ciliopathy mutants, which often exhibit severe cerebellar size
361 shrinkage, abnormal foliation and reduced GCP proliferation due to impaired Shh
362 signaling (16–18,64). In this regard, the postnatal Nes-CKO displayed profoundly mis-
363 patterned folia, and smaller cerebellum at later adult stage, similar to other ciliopathy
364 mutants. Nevertheless, in contrast to most ciliopathy mutants, Shh signaling in the
365 *Rab23*-KO mutant was not completely inhibited. Instead, there was a ligand-
366 independent upregulation of Shh pathway at basal level, which underlies the increase
367 in GCP proliferation and transiently enlarged cerebellum at earlier postnatal stages.
368 *Rab23* was known to influence *Gli2* and *Gli3* expression at the transcript level (65) and
369 it could also antagonize *Gli1*'s nuclear translocation and transcriptional activation in
370 cytosolic compartment in the absence of ligand stimulation (36). Given the ligand-
371 independent function of *Rab23* in Shh pathway, it is therefore plausible that the Shh
372 pathway in GCP became over-activated due to a basal increase in *Gli* activations in the
373 absence of *Rab23* function. However, limited by the incompetency to respond to Smo

374 activation from cell/cilium membrane (Fig 6F-G), Rab23-deficient GCP could not
375 reach or sustain the full capacity of ectopic Shh pathway activation, causing them less
376 susceptible to tumor formation as compared to other repressors such as *Ptch1* and *Sufu*
377 mutants that are not known to exhibit primary cilium defect.

378

379 Previous work has demonstrated that Rab23 maintains the overexpressed-Smo protein
380 turnover in the primary cilium of MDCK cells upon Shh stimulation (66), however, the
381 underlying mechanism, and how this regulation would affect Shh signaling output
382 remain elusive. Our data show that Rab23-depleted GCPs were less responsive to a
383 Smo agonist (SAG). As SAG activates Shh signaling pathway by facilitating Smo
384 translocation to the cilium axoneme, the compromised response observed in mutant
385 cells could possibly be caused by the lack of intact and functional primary cilium for Smo-
386 mediated signaling transduction, and/or impaired maintenance of Smo turnover in the
387 primary cilium of *Rab23*-KO GCP. Our data suggest that the cilium malformation could
388 be the underlying reason. However, the relatively short cilia in GCP cells was
389 technically difficult for detection or quantification of the cilium localization of Smo in
390 primary GCP. We are therefore not able to ascertain if the ciliary turnover/trafficking
391 of Smo protein is affected in the mutant GCP. Nevertheless, given its previous
392 implicated role on Smo protein turnover in MDCK cells (66), Rab23 could potentially
393 mediate the Smo recycling in primary cilium to influence Shh pathway.

394

395 Taken together, our findings suggest that Rab23 confers dual functions in regulating
396 Shh signaling and GCP proliferation; it potentiates primary cilium and Shh/Smo-
397 dependent signaling cascade, while antagonizing basal level Gli transcriptional
398 activation. Our data thus present a previously unappreciated aspect of Rab23 in

399 mediating Shh signaling upstream of Smo. This study sheds new light into the genetic
400 and mechanistic insights underpinning Shh signaling-mediated GCP proliferation and
401 cerebellar development.

402

403 **Materials and Methods**

404

405 *Animals.* *Rab23-floxed* animal was generated by Ozgene Pty Ltd. Conditional *Rab23-*
406 *floxed* allele was designed by flanking exon 4 for *Rab23* gene with loxP sites. Nestin-
407 Cre (Jackson Lab cat. no. 003771) was a kind gift from Shawn Je H.S. from Duke-Nus
408 Medical School. All animals were housed in Specific Pathogen Free (SPF) animal
409 facility at Duke-NUS Medical School, Singapore. All animal related procedures were
410 carried out in compliance to animal handling guidelines and protocol approved by
411 IACUC Singhealth, Singapore.

412

413 *Expression vectors.* For *in vitro* viral transduction assay, Rab23 over-expression or
414 cDNA were cloned into lentiviral pFUGW backbone. Wild-type (WT) Rab23
415 overexpression construct, previously described full-length Rab23 sequence (67) was
416 sub-cloned into pFUGW vector driven by Ubc promoter. All plasmids were amplified
417 according to the recommended protocol using Endofree® plasmid purification kit
418 (Qiagen, Germany).

419 *Viral transduction and culturing of mouse primary GCP.* For viral transduction of
420 primary GCP, self-inactivating murine lentiviruses were prepared according to
421 previously described protocol (42). GCP culture method was modified from standard
422 protocol. Briefly, P7 cerebellar tissues dissected were cut into small pieces and digested
423 in digestion buffer (EBSS / Papain, 1000 times dilution factor (Worthington

424 Biochemical Corporation cat#:3126) / 0.1 mg/ml DNaseI (Roche cat#:11284932001) /
425 5.5 mM cysteine-HCL) for 15 mins at 37 °C prior to dissociation into single cells.
426 Digestion was terminated by resuspension in 10 % FBS/culture medium. Suspension
427 culture was passed through 70 µm cell strainer (Corning cat#352350) to remove
428 undigested tissue clumps. Dissociated single-cell GCPs were plated on poly-D-lysine
429 (Sigma Aldrich cat#: P6407) coated culture plates at the desired cell densities in
430 Neurobasal (Gibco®, Life Technologies, USA) medium containing B27 supplement,
431 200uM GlutaMAX™-I (Gibco®, Life Technologies, USA), sodium pyruvate (1 mM),
432 penicilin/streptomycin and KCl (250 µM). Half of the culture medium was refreshed
433 every other day. Viral transduction was performed 2 to 3 hours after culture while
434 replacing fresh culture medium. The efficiencies of overexpression were validated by
435 real-time QPCR assay of DIV7 culture. For SAG stimulation, 0.2 µM of SAG (Cayman
436 Chemical, cat#: 11914-1) was added to the DIV 1 culture 24 hours prior to total RNA
437 extraction. Equal volume of DMSO was added as the untreated negative control group.
438 For Shh stimulation, 2 µg/ml of Shh (Stem Cell Technologies, cat#: 78065) was added
439 to the DIV 1 culture 24 hours prior to total RNA extraction.

440

441 ***EdU-pulse labelling assays.*** EdU labeling assay was carried out according to the
442 manufacturer's protocol. Click-iT ® EdU Alexa Fluor™ 647 Imaging Kit
443 (ThermoFisher Scientific, cat #: C10340). For GCP culture labeling, 10 µM Edu was
444 added to the culture and incubated for 3 hours before fixation. For E15.5 embryos
445 labelling, 0.25 mg EdU was injected intraperitoneally into the pregnant mice 2 hours
446 before fixing the embryo. For postnatal animals, 25ug EdU was injected
447 subcutaneously 2 hours prior to brain fixation.

448

449 ***Cryosectioning, immunohistochemistry and imaging.*** Mice were perfused with saline
450 followed by fixative in 4 % paraformaldehyde (Sigma Aldrich cat#:P6148) /
451 HistoChoice (Amresco, cat#: H120) mixture of 1:1 ratio, and whole brains extracted
452 were post-fix at 4 °C for 2 hours, saturated in 30 % sucrose in 0.12 M phosphate buffer
453 and subjected to cryosection at 20 µm thickness. All cerebellar tissues were sectioned
454 at sagittal angle and mounted on pre-coated glass slides (Superfrost® Plus,
455 Fisherbrand®). Mid-sagittal sections were selected for immunostaining. Antibodies and
456 the dilution factor used were: Pax6 (Covance, 1:1000), Nestin (Sigma, 1:800), NeuN
457 (Milipore, 1:800), GFAP (Milipore, 1:1000), Arl13b (Proteintech, 1:1000). For histo-
458 immunostaining, tissue sections were incubated at 100 °C for 10 mins in pH 6 10 mM
459 sodium citrate buffer with 0.05 % Tween-20 for antigen retrieval, washed twice with
460 phosphate buffer saline (PBS), blocked 1 hour in 1 % BSA/2 % horse serum/0.3 % Tx-
461 100 and incubated 4°C overnight with primary antibodies diluted in blocking buffer.
462 After 3 times of 5 minutes washes with PBS, tissue sections were incubated with
463 secondary antibodies (Alexa Fluor®, Life Technologies, USA) for 1 hour (hr) at room
464 temperature. Tissue sections were mounted in mounting media after 3 times PBS
465 washes. Fluorescence images were taken using Zeiss LSM710 confocal system.

466

467 ***Real-time quantitative PCR.*** Total RNA was extracted using Qiagen's RNeasy Mini
468 Kit. Equal amount of total RNAs from each sample were subjected to reverse
469 transcription to produce cDNA. Equal volume of cDNA was used to perform
470 quantitative PCR assay using SYBR® Select Master Mix (Applied Biosystems™
471 #4472908). Standard QPCR protocol was carried out according to manufacturer's
472 instruction manual. Primers used were: mouse GAPDH: F-5'-
473 TTCACCACCATGGAGAAGGC-3', R-5'- GGCATGGACTGTGGTCATGA-3';

474 mouse *Rab23*: F-5'-AGGCCTACTATCGAGGAGCC-3', R-5'-
475 TTAGCCTTTTGGCCAGTCCC-3'; mouse *Gli1*: F-5'-
476 CCCATAGGGTCTCGGGGTCTCAAAC-3', R-5'-
477 GGAGGACCTGCGGCTGACTGTGTA
478 A-3'; mouse *Gli2*: F-5'-CATGGTATCCCTAGCTCCTC-3', R-5'-
479 GATGGCATCAAAGTCAATCT-3'; mouse *Gli3*: F-5'-
480 CATGAACAGCCCTTTAAGAC-3', R-5'-TGATATGTGAGGTAGCACCA-3';
481 mouse *Ptch1*: F-5'-TGCTGTGCCTGTGGTCATCCTGATT-3', R-5'-
482 CAGAGCGAGCATAGCCCTGTGGTTC-3'; mouse *Atoh1*: F-5'-
483 AGTCAATGAAGTTGTTTCCC-3', R-5'-ACAGATACTCTTATCTGCCC-3';
484 mouse *Ki67*: F-5'-CATTGACCGCTCCTTTAGGTATGAAG-3', R-5'-
485 TTGGTATCTTGACCTTCCCCATCAG-3'.

486

487 **Acknowledgement**

488 We sincerely thank C.C. Hui and B.L Tang for sharing critical and constructive
489 comments and suggestions for the successful completion of this project. This study was
490 supported by the National Medical Research Council – Young Individual Research
491 Grant (NMRC/OFYIRG/0079/2018), HKBU Tier 1 and Tier 2 Start-up Grant (RG-
492 SGT2/18-19/SCI/009) to C.H.H; the National Medical Research Council –
493 Collaborative Research Grant (NMRC/CBRG/0094/2015) and Ministry of Education
494 (MOE) Tier 2 grant (MOE2015-T2-1-022) and Tier 3 grant (MOE2017-T3-1-002) to
495 E.L.G.

496

497

498 **Figure legends**

499

500 **Figure 1. Nestin-Cre-driven knock-out of *Rab23* causes expanded cerebellar size**
501 **and abnormal foliation.**

502 A) Representative whole mount images of control and Nes-CKO mutant brains
503 showing gross morphology of mouse cerebellum at P1, P4 and P15.

504 B) P4 cerebellar sizes as determined by measuring 2D surface area of cerebellum on
505 images captured at similar angle. Control, n = 6; CKO, n = 4 Statistical significance,
506 unpaired student t-test. P value ** ≤ 0.01 . Error bars depict \pm SE

507 C-D) Representative images showing H&E staining of control and Nes-CKO cerebellar
508 sagittal sections of P1 (C) and P4 (D) animals. Red arrows highlight morphological
509 changes in the external granule layer of Nes-CKO compared to the control.

510 E) Representative image showing whole brain of 2 months adult mice. Yellow asterisk
511 shows smaller cerebellum of Nes-CKO mutant compared to the control.

512 F) Representative images showing H&E staining of sagittal cerebellar sections of 10
513 months adult mice.

514

515 **Figure 2. KO of *Rab23* perturbs radial glial scaffold formation and causes partial**
516 **loss of cerebellar laminar structure**

517 A-B) Representative images showing immunostaining of Nestin (red) on P1 (A) and P4
518 (B) sagittal cerebellar tissue sections to illustrate radial glial scaffold.

519 C) Representative images showing immunostaining of GFAP (red) on P15 sagittal
520 cerebellar tissue sections to illustrate radial glial scaffold.

521 D) Representative images showing co-immunostaining of NeuN and GFAP on ten
522 months adult cerebellum to illustrate cerebellar cytoarchitecture, laminar layers and
523 glial cells.

524 D'-D'') Close up images showing NeuN-positive granule neurons and GFAP-positive
525 glial cells at the internal granule layer and pial surface.

526

527 **Figure 3. Depletion of Rab23 leads to GCP migration defect**

528 A) Representative images showing immunostaining of Pax6 on E15.5 sagittal sections
529 of cerebellar primordium to illustrate the GCPs residing in the EGL and early inward
530 migrating GCPs. White arrows show inward migration paths. EGL, external granular
531 layer; RL, rhombic lip

532 B) Quantification of the proportion of innervated Pax6+ GCPs against all Pax6-labelled
533 GCPs. 2 to 3 sections (~50-100 μ m apart) of the cerebellar primordium were counted
534 for each animal. Control, n = 3; CKO, n = 3. Statistical significance, unpaired student
535 t-test. P value * \leq 0.05. Error bars depict \pm SE

536 C) Representative image and graph showing two-hours EdU labelled progenitors in the
537 cerebellar primordium. Magenta arrows show migration paths of progenitors from
538 EGL, yellow arrows show migration paths of progenitors from VL. Control, n = 3;
539 CKO, n = 3. 2 to 3 sections (~50-100 μ m apart) were counted for each animal. Statistical
540 significance, unpaired student t-test. P value *** \leq 0.001. Error bars depict \pm SE

541 D) Representative images showing cerebellar lobules of 48 hours Edu-labelled cells
542 from P5-P7 to illustrate proportions of cells innervated the IGL after 48 hours of pulse-
543 chase labeling. EGL, external granular layer; ML, molecular layer; ICL, internal
544 granule layer.

545 E) Quantification of the proportion of Edu-labelled cells in each laminar layer as
546 indicated. Control, n = 3; CKO, n = 3. Statistical significance, two-way ANOVA,
547 Bonferroni posttests. P value *** \leq 0.001, ** \leq 0.01, * \leq 0.05. Error bars depict \pm SE

548

549 **Figure 4. *Rab23*-deficient cerebellum exhibited thickened EGL and elevated GCP**
550 **proliferation**

551 A-B) Representative images showing co-immunostaining of Pax6 (green) and
552 Calbindin (red) on P1 sagittal sections of cerebellum to illustrate the GCPs and Purkinje
553 cells layers. Asterisks show a thickened EGL layer in Nes-CKO cerebellum compared
554 to the control.

555 C-D) Representative images showing two-hours EdU labelled dividing progenitors in
556 the E15.5 (C) and P4 (D) cerebellum. Double headed arrows highlight expanded pools
557 of dividing cells in the Nes-CKO EGL as compared to the control counterparts.

558 E) Quantification of the percentages of 2 hours Edu-labelled proliferative cells in the
559 EGL at E15.5. 2 sections (~100 μm apart) of the cerebellar primordium were counted
560 for each animal. Control, n = 3; CKO n = 3. Statistical significance, unpaired student t-
561 test. P value *** ≤ 0.001 . Error bars depict $\pm\text{SE}$

562 F) Graphs illustrating the fold change of the gene expression levels of E15.5 cerebellar
563 tissues quantified by real-time quantitative PCR. Control, n = 4; CKO n = 4. Nes-CKO
564 values were normalized to its respective control group. Statistical significance, unpaired
565 student t-test. P value *** ≤ 0.001 . Error bars depict $\pm\text{SE}$

566

567 **Figure 5. *Shh* activity is differentially perturbed in the embryonic and postnatal**
568 **cerebellar tissues.**

569 A) Graphs illustrating the fold change of the gene expression levels of E15.5 cerebellar
570 tissues quantified by real-time quantitative PCR. Control, n = 4; CKO n = 4. Nes-CKO
571 values were normalized to its respective control group. Statistical significance, unpaired
572 student t-test. P value ** ≤ 0.01 . Error bars depict $\pm\text{SE}$. n.s., not significant.

573 B) Graphs illustrating the fold change of the gene expression levels of P15 cerebellar
574 tissues quantified by real-time quantitative PCR. Nes-CKO values were normalized to
575 its respective control group. Control, n = 3; CKO n = 4. Statistical significance,
576 unpaired student t-test. P value *** ≤ 0.001 . Error bars depict \pm SE. n.s., not significant.
577 C) Graphs illustrating the basal level *Gli1* expression profiles of E15.5 and P15
578 cerebellar tissues quantified by real-time quantitative PCR. E15.5 Control, n = 4; CKO
579 n = 4; P15 Control, n = 3; CKO n = 4. Statistical significance, one-way ANOVA,
580 Bonferroni's Multiple Comparison Test. P value *** ≤ 0.0001 . Error bars depict \pm SE.
581 n.s., not significant.

582

583 **Figure 6. *Rab23* regulates ciliogenesis and Shh signaling in the GCPs.**

584 A) Graphs showing gene expression levels of P7 GCPs primary cultures harvested at
585 DIV 7. Lentiviral carrying the over-expression constructs as indicated were transduced
586 into the primary cultures at Day 0, 2 to 3 hours after seeding cells. Quantifications
587 depict 4 independent experiments. Statistical significance, one-way ANOVA,
588 Bonferroni's Multiple Comparison Test. P value *** ≤ 0.0001 ; ** ≤ 0.01 , * ≤ 0.05 . Error
589 bars depict \pm SE.

590 B-C) Representative images (B) and graph (C) showing three-hours EdU labelled
591 (magenta; blue: DAPI) dividing progenitors in P7 GCPs primary cultures of each
592 indicated groups fixed at DIV 7. Cell proliferation was determined by the percentages
593 of Edu-labelled cells out of total number of DAP-positive nuclei in each image taken.
594 For quantification of each batch, 3 fluorescence images were randomly taken from each
595 respective group as indicated. Quantifications depict 3 independent experiments.
596 Statistical significance, one-way ANOVA, Bonferroni's Multiple Comparison Test. P
597 value *** ≤ 0.0001 ; ** ≤ 0.01 . Error bars depict \pm SE.

598 D) Quantification of the percentages of ciliation in P7 GCPs primary cultures at DIV7
599 determined by counting the number of cells bearing Arl13B-labelled primary cilium
600 against all DAPI-positive nuclei in each image taken. For quantification of each batch,
601 3 fluorescence images were randomly taken from each respective group as indicated.
602 Quantifications depict 3 independent experiments. Statistical significance, one-way
603 ANOVA, Bonferroni's Multiple Comparison Test. P value *** ≤ 0.0001 ; ** ≤ 0.01 .
604 Error bars depict \pm SE.

605 E) Representative images showing immunostaining of Arl13B on E15.5 (top) and P15
606 (bottom) sagittal sections to illustrate the primary cilia of GCPs residing in the EGL.
607 EGL, external granular layer; ML, molecular layer.

608 F-G) Graphs showing gene expression levels of P7 GCPs primary cultures treated with
609 Shh (F) and SAG (G) on DIV 1 respectively. Total RNAs were extracted from DIV 2
610 culture, 24 hours after the respective treatments. Quantifications depict double delta Ct
611 values of 3 independent experiments. Delta Ct values of the treated groups were
612 normalized to its respective untreated group, which gave double delta Ct values as
613 plotted. Statistical significance, unpaired student t-test. P value *** ≤ 0.0001 ; ** ≤ 0.01 .
614 Error bars depict \pm SE.

615 **References**

- 616 1. Wallace VA. Purkinje-cell-derived Sonic hedgehog regulates granule neuron
617 precursor cell proliferation in the developing mouse cerebellum [Internet]. Vol.
618 9, *Current Biology*. Elsevier; 1999. p. 445–8. Available from:
619 [http://www.cell.com/current-biology/abstract/S0960-9822\(99\)80195-X](http://www.cell.com/current-biology/abstract/S0960-9822(99)80195-X)
- 620 2. Wechsler-Reya RJ, Scott MP. Control of neuronal precursor proliferation in the
621 cerebellum by sonic hedgehog. *Neuron*. 1999;22(1):103–14.
- 622 3. Gao W-Q, Heintz N, Hatten ME. Cerebellar granule cell neurogenesis is
623 regulated by cell-cell interactions in vitro. *Neuron* [Internet]. 1991
624 May;6(5):705–15. Available from:
625 <http://linkinghub.elsevier.com/retrieve/pii/089662739190168Y>
- 626 4. Basson MA, Wingate RJ. Congenital hypoplasia of the cerebellum:
627 developmental causes and behavioral consequences. *Front Neuroanat*
628 [Internet]. 2013 Sep 3 [cited 2018 Nov 23];7:29. Available from:
629 <http://www.ncbi.nlm.nih.gov/pubmed/24027500>
- 630 5. Roussel MF, Hatten ME. Cerebellum development and medulloblastoma. *Curr*
631 *Top Dev Biol* [Internet]. 2011;94:235–82. Available from:
632 <http://linkinghub.elsevier.com/retrieve/pii/B9780123809162000085>
- 633 6. Dahmane N, Ruiz i Altaba A. Sonic hedgehog regulates the growth and
634 patterning of the cerebellum. *Development* [Internet]. 1999 Jun;126(14):3089–
635 100. Available from: <http://www.ncbi.nlm.nih.gov/pubmed/10375501>
- 636 7. Lewis PM, Gritli-Linde A, Smeyne R, Kottmann A, McMahon AP. Sonic
637 hedgehog signaling is required for expansion of granule neuron precursors and
638 patterning of the mouse cerebellum. *Dev Biol* [Internet]. 2004 Jun;270(2):393–
639 410. Available from:
640 <http://linkinghub.elsevier.com/retrieve/pii/S0012160604001939>
- 641 8. Dey J, Ditzler S, Knoblauch SE, Hatton BA, Schelter JM, Cleary MA, et al. A
642 Distinct Smoothed Mutation Causes Severe Cerebellar Developmental
643 Defects and Medulloblastoma in a Novel Transgenic Mouse Model. *Mol Cell*
644 *Biol* [Internet]. 2012;32(20):4104–15. Available from:
645 <http://mcb.asm.org/cgi/doi/10.1128/MCB.00862-12>
- 646 9. Dong J, Gailani MR, Pomeroy SL, Reardon D, Bale AE. Identification
647 of PATCHED mutations in medulloblastomas by direct sequencing [Internet].
648 Vol. 16, *Hum. Mutat*. 2000. p. 89–90. Available from:
649 [http://doi.wiley.com/10.1002/1098-](http://doi.wiley.com/10.1002/1098-1004%28200007%2916%3A1%3C89%3A%3AAID-HUMU18%3E3.0.CO%3B2-7)
650 [1004%28200007%2916%3A1%3C89%3A%3AAID-](http://doi.wiley.com/10.1002/1098-1004%28200007%2916%3A1%3C89%3A%3AAID-HUMU18%3E3.0.CO%3B2-7)
651 [HUMU18%3E3.0.CO%3B2-7](http://doi.wiley.com/10.1002/1098-1004%28200007%2916%3A1%3C89%3A%3AAID-HUMU18%3E3.0.CO%3B2-7)
- 652 10. Taylor MD, Liu L, Raffel C, Hui C, Mainprize TG, Zhang X, et al. Mutations
653 in SUFU predispose to medulloblastoma. *Nat Genet* [Internet]. 2002 Jul
654 17;31(3):306–10. Available from: <http://www.nature.com/articles/ng916z>
- 655 11. Raffel C, Jenkins RB, Frederick L, Hebrink D, Alderete B, Fults DW, et al.
656 Sporadic medulloblastomas contain PTCH mutations. *Cancer Res* [Internet].
657 1997 Mar 1;57(5):842–5. Available from:
658 <http://www.ncbi.nlm.nih.gov/pubmed/9041183>
- 659 12. Begemann M, Waszak SM, Robinson GW, Jäger N, Sharma T, Knopp C, et al.
660 Germline GPR161 mutations predispose to pediatric medulloblastoma. *J Clin*
661 *Oncol* [Internet]. 2020 Jan 1 [cited 2020 Mar 9];38(1):43–50. Available from:
662 <http://ascopubs.org/doi/10.1200/JCO.19.00577>
- 663 13. Tukachinsky H, Lopez L V, Salic A. A mechanism for vertebrate Hedgehog
664 signaling: recruitment to cilia and dissociation of SuFu-Gli protein complexes

- 665 [Internet]. Vol. 191, *The Journal of Cell Biology*. 2010. p. 415–28. Available
666 from: <http://jcb-dataviewer.rupress.org/jcb/doi/10.1083/jcb.201004108>
- 667 14. Haycraft CJ, Banizs B, Aydin-Son Y, Zhang Q, Michaud EJ, Yoder BK. Gli2
668 and Gli3 localize to cilia and require the intraflagellar transport protein polaris
669 for processing and function. [Internet]. Vol. 1, *PLoS Genet*. 2005. p. e53.
670 Available from:
671 [http://eutils.ncbi.nlm.nih.gov/entrez/eutils/elink.fcgi?dbfrom=pubmed&id](http://eutils.ncbi.nlm.nih.gov/entrez/eutils/elink.fcgi?dbfrom=pubmed&id=16254602&retmode=ref&cmd=prlinks)
672 [=16254602&retmode=ref&cmd=prlinks](http://eutils.ncbi.nlm.nih.gov/entrez/eutils/elink.fcgi?dbfrom=pubmed&id=16254602&retmode=ref&cmd=prlinks)
- 673 15. Wong SY, Seol AD, So P-L, Ermilov AN, Bichakjian CK, Epstein EH, et al.
674 Primary cilia can both mediate and suppress Hedgehog pathway–dependent
675 tumorigenesis. *Nat Med* [Internet]. 2009 Sep 23;15(9):1055–61. Available
676 from: <http://www.nature.com/articles/nm.2011>
- 677 16. Spassky N, Han Y-G, Aguilar A, Strehl L, Besse L, Laclef C, et al. Primary
678 cilia are required for cerebellar development and Shh-dependent expansion of
679 progenitor pool. *Dev Biol* [Internet]. 2008 May;317(1):246–59. Available
680 from: <http://linkinghub.elsevier.com/retrieve/pii/S0012160608001395>
- 681 17. Chizhikov V V., Davenport J, Zhang Q, Shih EK, Cabello OA, Fuchs JL, et al.
682 Cilia proteins control cerebellar morphogenesis by promoting expansion of the
683 granule progenitor pool. *J Neurosci* [Internet]. 2007 Sep 5;27(36):9780–9.
684 Available from: <http://www.ncbi.nlm.nih.gov/pubmed/17804638>
- 685 18. Han YG, Kim HJ, Dlugosz AA, Ellison DW, Gilbertson RJ, Alvarez-Buylla A.
686 Dual and opposing roles of primary cilia in medulloblastoma development. *Nat*
687 *Med* [Internet]. 2009;15(9):1062–5. Available from:
688 <http://dx.doi.org/10.1038/nm.2020>
- 689 19. Bay SN, Long AB, Caspary T. Disruption of the ciliary GTPase Arl13b
690 suppresses Sonic hedgehog overactivation and inhibits medulloblastoma
691 formation. *Proc Natl Acad Sci* [Internet]. 2018 Feb 13 [cited 2019 Jan
692 5];115(7):1570–5. Available from:
693 www.pnas.org/cgi/doi/10.1073/pnas.1706977115
- 694 20. Gajjar A, Stewart CF, Ellison DW, Kaste S, Kun LE, Packer RJ, et al. Phase I
695 Study of Vismodegib in Children with Recurrent or Refractory
696 Medulloblastoma: A Pediatric Brain Tumor Consortium Study. *Clin Cancer*
697 *Res* [Internet]. 2013 Nov 15 [cited 2018 Nov 28];19(22):6305–12. Available
698 from: <http://www.ncbi.nlm.nih.gov/pubmed/24077351>
- 699 21. Guo A, Wang T, Ee LN, Aulia S, Kooi HC, Teng FYH, et al. Open brain gene
700 product Rab23: Expression pattern in the adult mouse brain and functional
701 characterization. *J Neurosci Res*. 2006;
- 702 22. Alessandri J-L, Dagoneau N, Laville J-M, Baruteau J, Hébert J-C, Cormier-
703 Daire V. RAB23 mutation in a large family from Comoros Islands with
704 Carpenter syndrome. [Internet]. Vol. 152A, *Am. J. Med. Genet*. 2010. p. 982–
705 6. Available from:
706 [http://eutils.ncbi.nlm.nih.gov/entrez/eutils/elink.fcgi?dbfrom=pubmed&id](http://eutils.ncbi.nlm.nih.gov/entrez/eutils/elink.fcgi?dbfrom=pubmed&id=20358613&retmode=ref&cmd=prlinks)
707 [=20358613&retmode=ref&cmd=prlinks](http://eutils.ncbi.nlm.nih.gov/entrez/eutils/elink.fcgi?dbfrom=pubmed&id=20358613&retmode=ref&cmd=prlinks)
- 708 23. Jenkins D, Seelow D, Jehee FS, Perlyn CA, Alonso LG, Bueno DF, et al.
709 RAB23 mutations in Carpenter syndrome imply an unexpected role for
710 hedgehog signaling in cranial-suture development and obesity. [Internet]. Vol.
711 80, *Am. J. Hum. Genet*. 2007. p. 1162–70. Available from:
712 [http://eutils.ncbi.nlm.nih.gov/entrez/eutils/elink.fcgi?dbfrom=pubmed&id](http://eutils.ncbi.nlm.nih.gov/entrez/eutils/elink.fcgi?dbfrom=pubmed&id=17503333&retmode=ref&cmd=prlinks)
713 [=17503333&retmode=ref&cmd=prlinks](http://eutils.ncbi.nlm.nih.gov/entrez/eutils/elink.fcgi?dbfrom=pubmed&id=17503333&retmode=ref&cmd=prlinks)
- 714 24. Haye D, Collet C, Sembely-Taveau C, Haddad G, Denis C, Soulé N, et al.

- 715 Prenatal findings in carpenter syndrome and a novel mutation in RAB23.
716 [Internet]. Vol. 164A, *Am. J. Med. Genet.* 2014. p. 2926–30. Available from:
717 [http://eutils.ncbi.nlm.nih.gov/entrez/eutils/elink.fcgi?dbfrom=pubmed&id](http://eutils.ncbi.nlm.nih.gov/entrez/eutils/elink.fcgi?dbfrom=pubmed&id=25168863&retmode=ref&cmd=prlinks)
718 [=25168863&retmode=ref&cmd=prlinks](http://eutils.ncbi.nlm.nih.gov/entrez/eutils/elink.fcgi?dbfrom=pubmed&id=25168863&retmode=ref&cmd=prlinks)
- 719 25. Tarhan E, Oğuz H, Şafak MA, Samim E. The Carpenter syndrome phenotype.
720 *Int J Pediatr Otorhinolaryngol.* 2004;68(3):353–7.
- 721 26. Balci S, Onol B, Eryilmaz M, Haytöglu T. A case of Carpenter syndrome
722 diagnosed in a 20-week-old fetus with postmortem examination. *Clin Genet.*
723 1997;51(6):412–6.
- 724 27. Bersani G, Maddalena F, Pasquini M, Orlandi V, Pancheri P. Association of
725 schizophrenia and Carpenter syndrome. *Acta Neuropsychiatr* [Internet]. 2003
726 Oct 24;15(05):304–5. Available from:
727 [https://www.cambridge.org/core/product/identifier/S0924270800004373/type/j](https://www.cambridge.org/core/product/identifier/S0924270800004373/type/journal_article)
728 [ournal_article](https://www.cambridge.org/core/product/identifier/S0924270800004373/type/journal_article)
- 729 28. Ivaniutsin U, Chen Y, Mason JO, Price DJ, Pratt T. Adenomatous polyposis
730 coli is required for early events in the normal growth and differentiation of the
731 developing cerebral cortex. [Internet]. Vol. 4, *Neural Dev.* 2009. p. 3.
732 Available from:
733 [http://eutils.ncbi.nlm.nih.gov/entrez/eutils/elink.fcgi?dbfrom=pubmed&id](http://eutils.ncbi.nlm.nih.gov/entrez/eutils/elink.fcgi?dbfrom=pubmed&id=19149881&retmode=ref&cmd=prlinks)
734 [=19149881&retmode=ref&cmd=prlinks](http://eutils.ncbi.nlm.nih.gov/entrez/eutils/elink.fcgi?dbfrom=pubmed&id=19149881&retmode=ref&cmd=prlinks)
- 735 29. Taravath S, Tonsgard JH. Cerebral malformations in Carpenter syndrome.
736 *Pediatr Neurol* [Internet]. 1993 May 1 [cited 2018 Nov 28];9(3):230–4.
737 Available from: <http://www.ncbi.nlm.nih.gov/pubmed/8352858>
- 738 30. Eggenschwiler JT, Espinoza E, Anderson K V. Rab23 is an essential negative
739 regulator of the mouse Sonic hedgehog signalling pathway. [Internet]. Vol.
740 412, *Nature.* 2001. p. 194–8. Available from:
741 [http://eutils.ncbi.nlm.nih.gov/entrez/eutils/elink.fcgi?dbfrom=pubmed&id](http://eutils.ncbi.nlm.nih.gov/entrez/eutils/elink.fcgi?dbfrom=pubmed&id=11449277&retmode=ref&cmd=prlinks)
742 [=11449277&retmode=ref&cmd=prlinks](http://eutils.ncbi.nlm.nih.gov/entrez/eutils/elink.fcgi?dbfrom=pubmed&id=11449277&retmode=ref&cmd=prlinks)
- 743 31. Eggenschwiler JT, Bulgakov O V, Qin J, Li T, Anderson K V. Mouse Rab23
744 regulates Hedgehog signaling from Smoothed to Gli proteins [Internet]. Vol.
745 290, *Developmental Biology.* 2006. p. 1–12. Available from:
746 <http://linkinghub.elsevier.com/retrieve/pii/S0012160605006299>
- 747 32. Svärd J, Heby-Henricson K, Henricson KH, Persson-Lek M, Rozell B, Lauth
748 M, et al. Genetic elimination of Suppressor of fused reveals an essential
749 repressor function in the mammalian Hedgehog signaling pathway. [Internet].
750 Vol. 10, *Developmental Cell.* 2006. p. 187–97. Available from:
751 [http://www.ncbi.nlm.nih.gov/sites/entrez?Db=pubmed&Cmd=ShowDetail](http://www.ncbi.nlm.nih.gov/sites/entrez?Db=pubmed&Cmd=ShowDetailView&TermToSearch=16459298&ordinalpos=3&itool=EntrezSystem2.PEntrez.Pubmed.Pubmed_ResultsPanel.Pubmed_RVDocSum)
752 [View&TermToSearch=16459298&ordinalpos=3&itool=EntrezS](http://www.ncbi.nlm.nih.gov/sites/entrez?Db=pubmed&Cmd=ShowDetailView&TermToSearch=16459298&ordinalpos=3&itool=EntrezSystem2.PEntrez.Pubmed.Pubmed_ResultsPanel.Pubmed_RVDocSum)
753 [ystem2.PEntrez.Pubmed.Pubmed_ResultsPanel.Pubmed_RVDocSum](http://www.ncbi.nlm.nih.gov/sites/entrez?Db=pubmed&Cmd=ShowDetailView&TermToSearch=16459298&ordinalpos=3&itool=EntrezSystem2.PEntrez.Pubmed.Pubmed_ResultsPanel.Pubmed_RVDocSum)
- 754 33. Cooper AF. Cardiac and CNS defects in a mouse with targeted disruption of
755 suppressor of fused [Internet]. Vol. 132, *Development.* 2005. p. 4407–17.
756 Available from: <http://dev.biologists.org/cgi/doi/10.1242/dev.02021>
- 757 34. Jeong J. Growth and pattern of the mammalian neural tube are governed by
758 partially overlapping feedback activities of the hedgehog antagonists patched 1
759 and Hhip1. *Development* [Internet]. 2004 Dec 2;132(1):143–54. Available
760 from: <http://dev.biologists.org/cgi/doi/10.1242/dev.01566>
- 761 35. Boehlke C, Bashkurov M, Buescher A, Krick T, John A-K, Nitschke R, et al.
762 Differential role of Rab proteins in ciliary trafficking: Rab23 regulates
763 smoothed levels. *J Cell Sci* [Internet]. 2010 May 1 [cited 2018 Nov
764 22];123(Pt 9):1460–7. Available from:

- 765 <http://www.ncbi.nlm.nih.gov/pubmed/20375059>
766 36. Chi S, Xie G, Liu H, Chen K, Zhang X, Li C, et al. Rab23 negatively regulates
767 Gli1 transcriptional factor in a Su(Fu)-dependent manner. *Cell Signal*
768 [Internet]. 2012 Jun;24(6):1222–8. Available from:
769 <https://linkinghub.elsevier.com/retrieve/pii/S0898656812000599>
770 37. Yoshimura S i, Egerer J, Fuchs E, Haas AK, Barr FA. Functional dissection of
771 Rab GTPases involved in primary cilium formation [Internet]. Vol. 178, *The*
772 *Journal of Cell Biology*. 2007. p. 363–9. Available from:
773 <http://www.jcb.org/cgi/doi/10.1083/jcb.200703047>
774 38. Gerondopoulos A, Strutt H, Stevenson NL, Sobajima T, Levine TP, Stephens
775 DJ, et al. Planar Cell Polarity Effector Proteins Inturned and Fuzzy Form a
776 Rab23 GEF Complex. *Curr Biol* [Internet]. 2019 Oct;29(19):3323–3330.e8.
777 Available from:
778 <https://linkinghub.elsevier.com/retrieve/pii/S0960982219310164>
779 39. Fuller K, O’Connell JT, Gordon J, Mauti O, Eggenschwiler J. Rab23
780 regulates Nodal signaling in vertebrate left-right patterning independently of
781 the Hedgehog pathway. [Internet]. Vol. 391, *Developmental Biology*. 2014. p.
782 182–95. Available from:
783 [http://eutils.ncbi.nlm.nih.gov/entrez/eutils/elink.fcgi?dbfrom=pubmed&id](http://eutils.ncbi.nlm.nih.gov/entrez/eutils/elink.fcgi?dbfrom=pubmed&id=24780629&retmode=ref&cmd=prlinks)
784 [=24780629&retmode=ref&cmd=prlinks](http://eutils.ncbi.nlm.nih.gov/entrez/eutils/elink.fcgi?dbfrom=pubmed&id=24780629&retmode=ref&cmd=prlinks)
785 40. Lim YS, Tang BL. A role for Rab23 in the trafficking of Kif17 to the primary
786 cilium. [Internet]. Vol. 128, *J. Cell. Sci*. 2015. p. 2996–3008. Available from:
787 [http://eutils.ncbi.nlm.nih.gov/entrez/eutils/elink.fcgi?dbfrom=pubmed&id](http://eutils.ncbi.nlm.nih.gov/entrez/eutils/elink.fcgi?dbfrom=pubmed&id=26136363&retmode=ref&cmd=prlinks)
788 [=26136363&retmode=ref&cmd=prlinks](http://eutils.ncbi.nlm.nih.gov/entrez/eutils/elink.fcgi?dbfrom=pubmed&id=26136363&retmode=ref&cmd=prlinks)
789 41. Leaf A, Von Zastrow M. Dopamine receptors reveal an essential role of IFT-B,
790 KIF17, and Rab23 in delivering specific receptors to primary cilia. [Internet].
791 Vol. 4, *Elife*. 2015. Available from:
792 [http://eutils.ncbi.nlm.nih.gov/entrez/eutils/elink.fcgi?dbfrom=pubmed&id](http://eutils.ncbi.nlm.nih.gov/entrez/eutils/elink.fcgi?dbfrom=pubmed&id=26182404&retmode=ref&cmd=prlinks)
793 [=26182404&retmode=ref&cmd=prlinks](http://eutils.ncbi.nlm.nih.gov/entrez/eutils/elink.fcgi?dbfrom=pubmed&id=26182404&retmode=ref&cmd=prlinks)
794 42. Hor CHH, Goh ELK. Rab23 Regulates Radial Migration of Projection Neurons
795 via N-cadherin. *Cereb Cortex* [Internet]. 2018 Apr 1;28(4):1516–31. Available
796 from: <https://academic.oup.com/cercor/article/28/4/1516/4840630>
797 43. Xu H, Yang Y, Tang X, Zhao M, Liang F, Xu P, et al. Bergmann Glia Function
798 in Granule Cell Migration During Cerebellum Development. *Mol Neurobiol*
799 [Internet]. 2013 Apr 19 [cited 2018 Nov 16];47(2):833–44. Available from:
800 [https://link-springer-](https://link-springer-com.libproxy1.nus.edu.sg/content/pdf/10.1007%2Fs12035-013-8405-y.pdf)
801 [com.libproxy1.nus.edu.sg/content/pdf/10.1007%2Fs12035-013-8405-y.pdf](https://link-springer-com.libproxy1.nus.edu.sg/content/pdf/10.1007%2Fs12035-013-8405-y.pdf)
802 44. Sidman RL, Rakic P. Neuronal migration, with special reference to developing
803 human brain: a review. *Brain Res* [Internet]. 1973 Nov;62(1):1–35. Available
804 from: <http://linkinghub.elsevier.com/retrieve/pii/0006899373906173>
805 45. Yue Q. PTEN deletion in Bergmann glia leads to premature differentiation and
806 affects laminar organization. *Development* [Internet]. 2005;132(14):3281–91.
807 Available from: <http://dev.biologists.org/cgi/doi/10.1242/dev.01891>
808 46. Chung S, Kim C, Jung Y, Lee N, Jeong Y. Early cerebellar granule cell
809 migration in the mouse embryonic development. *Cell*. 2010;86–95.
810 47. Kim JYH, Nelson AL, Algon SA, Graves O, Sturla LM, Goumnerova LC, et al.
811 Medulloblastoma tumorigenesis diverges from cerebellar granule cell
812 differentiation in patched heterozygous mice. *Dev Biol* [Internet]. 2003
813 Nov;263(1):50–66. Available from:
814 <http://linkinghub.elsevier.com/retrieve/pii/S0012160603004342>

- 815 48. Yoshioka K. Control of granule cell precursor proliferation in the developing
816 cerebellum and in medulloblastoma. *Biomedical Reviews*. 2005.
- 817 49. Roussel MF, Hatten ME. Cerebellum development and medulloblastoma. *Curr*
818 *Top Dev Biol* [Internet]. 2011;94:235–82. Available from:
819 <http://www.ncbi.nlm.nih.gov/pubmed/21295689>
- 820 50. Evans TM, Simpson F, Parton RG, Wicking C. Characterization of Rab23, a
821 Negative Regulator of Sonic Hedgehog Signaling. In: *Methods in enzymology*
822 [Internet]. 2005. p. 759–77. Available from:
823 <http://www.ncbi.nlm.nih.gov/pubmed/16473637>
- 824 51. Corrales JD. Spatial pattern of sonic hedgehog signaling through Gli genes
825 during cerebellum development. *Development* [Internet]. 2004;131(22):5581–
826 90. Available from: <http://dev.biologists.org/cgi/doi/10.1242/dev.01438>
- 827 52. Lewis PM, Gritli-Linde A, Smeyne R, Kottmann A, McMahon AP. Sonic
828 hedgehog signaling is required for expansion of granule neuron precursors and
829 patterning of the mouse cerebellum. [Internet]. Vol. 270, *Developmental*
830 *Biology*. 2004. p. 393–410. Available from:
831 [http://eutils.ncbi.nlm.nih.gov/entrez/eutils/elink.fcgi?dbfrom=pubmed&id](http://eutils.ncbi.nlm.nih.gov/entrez/eutils/elink.fcgi?dbfrom=pubmed&id=15183722&retmode=ref&cmd=prlinks)
832 [=15183722&retmode=ref&cmd=prlinks](http://eutils.ncbi.nlm.nih.gov/entrez/eutils/elink.fcgi?dbfrom=pubmed&id=15183722&retmode=ref&cmd=prlinks)
- 833 53. Lee J, Platt KA, Censullo P, Ruiz i Altaba A. Gli1 is a target of Sonic
834 hedgehog that induces ventral neural tube development. *Development*
835 [Internet]. 1997 Jul;124(13):2537–52. Available from:
836 <http://www.ncbi.nlm.nih.gov/pubmed/9216996>
- 837 54. Bai CB, Joyner AL. Gli1 can rescue the in vivo function of Gli2. *Development*
838 [Internet]. 2001 Dec;128(24):5161–72. Available from:
839 <http://www.ncbi.nlm.nih.gov/pubmed/11748151>
- 840 55. Bai CB, Stephen D, Joyner AL. All mouse ventral spinal cord patterning by
841 hedgehog is Gli dependent and involves an activator function of Gli3. *Dev Cell*
842 [Internet]. 2004 Jan;6(1):103–15. Available from:
843 <http://linkinghub.elsevier.com/retrieve/pii/S1534580703003940>
- 844 56. Yoshimura S, Egerer J, Fuchs E, Haas AK, Barr FA. Functional dissection of
845 Rab GTPases involved in primary cilium formation. *J Cell Biol* [Internet]. 2007
846 Jul 30;178(3):363–9. Available from:
847 <http://www.jcb.org/lookup/doi/10.1083/jcb.200703047>
- 848 57. Butts T, Green MJ, Wingate RJT. Development of the cerebellum: simple steps
849 to make a “little brain.” *Development* [Internet]. 2014;141(21):4031–41.
850 Available from: <http://dev.biologists.org/cgi/doi/10.1242/dev.106559>
- 851 58. Wallace VA. Purkinje-cell-derived Sonic hedgehog regulates granule neuron
852 precursor cell proliferation in the developing mouse cerebellum. *Curr Biol*
853 [Internet]. 1999 Apr 22;9(8):445–8. Available from:
854 <http://linkinghub.elsevier.com/retrieve/pii/S096098229980195X>
- 855 59. Miyazawa K, Himi T, Garcia V, Yamagishi H, Sato S, Ishizaki Y. A role for
856 p27/Kip1 in the control of cerebellar granule cell precursor proliferation. *J*
857 *Neurosci*. 2000;20(15):5756–63.
- 858 60. Hor CHH, Tang BL, Goh ELK. Rab23 and developmental disorders. *Rev*
859 *Neurosci* [Internet]. 2018 Nov 27;29(8):849–60. Available from:
860 [http://www.degruyter.com/view/j/revneuro.2018.29.issue-8/revneuro-2017-](http://www.degruyter.com/view/j/revneuro.2018.29.issue-8/revneuro-2017-0110/revneuro-2017-0110.xml)
861 [0110/revneuro-2017-0110.xml](http://www.degruyter.com/view/j/revneuro.2018.29.issue-8/revneuro-2017-0110/revneuro-2017-0110.xml)
- 862 61. Begemann M, Waszak SM, Robinson GW, Jäger N, Sharma T, Knopp C, et al.
863 Germline GPR161 mutations predispose to pediatric medulloblastoma. *J Clin*
864 *Oncol*. 2020 Jan;38(1):43–50.

- 865 62. Zurawel RH, Allen C, Wechsler-Reya R, Scott MP, Raffel C. Evidence that
866 haploinsufficiency of Ptc leads to medulloblastoma in mice. *Genes,*
867 *Chromosom Cancer.* 2000 May 1;28(1):77–81.
- 868 63. Kimura H, Stephen D, Joyner A, Curran T. Gli1 is important for
869 medulloblastoma formation in Ptc1+/- mice. *Oncogene* [Internet]. 2005 Jun
870 4;24(25):4026–36. Available from: <http://www.nature.com/articles/1208567>
- 871 64. Barakat MT, Humke EW, Scott MP. Kif3a is necessary for initiation and
872 maintenance of medulloblastoma. *Carcinogenesis.* 2013;34(6):1382–92.
- 873 65. Eggenschwiler JT, Bulgakov O V., Qin J, Li T, Anderson K V. Mouse Rab23
874 regulates Hedgehog signaling from Smoothed to Gli proteins. *Dev Biol*
875 [Internet]. 2006 Feb 1 [cited 2018 Nov 21];290(1):1–12. Available from:
876 <https://www.sciencedirect.com/science/article/pii/S0012160605006299?via%3>
877 *Dihub*
- 878 66. Boehlke C, Bashkurov M, Buescher A, Krick T, John A-K, Nitschke R, et al.
879 Differential role of Rab proteins in ciliary trafficking: Rab23 regulates
880 smoothed levels. *J Cell Sci* [Internet]. 2010 May 1;123(Pt 9):1460–7.
881 Available from: <http://www.ncbi.nlm.nih.gov/pubmed/20375059>
- 882 67. Guo A, Wang T, Ng EL, Aulia S, Chong KH, Teng FYH, et al. Open brain
883 gene product Rab23: expression pattern in the adult mouse brain and functional
884 characterization. *J Neurosci Res* [Internet]. 2006;83(6):1118–27. Available
885 from:
886 [http://eutils.ncbi.nlm.nih.gov/entrez/eutils/elink.fcgi?dbfrom=pubmed&id](http://eutils.ncbi.nlm.nih.gov/entrez/eutils/elink.fcgi?dbfrom=pubmed&id=16463280&retmode=ref&cmd=prlinks)
887 [=16463280&retmode=ref&cmd=prlinks](http://eutils.ncbi.nlm.nih.gov/entrez/eutils/elink.fcgi?dbfrom=pubmed&id=16463280&retmode=ref&cmd=prlinks)
888
889

Figure 1

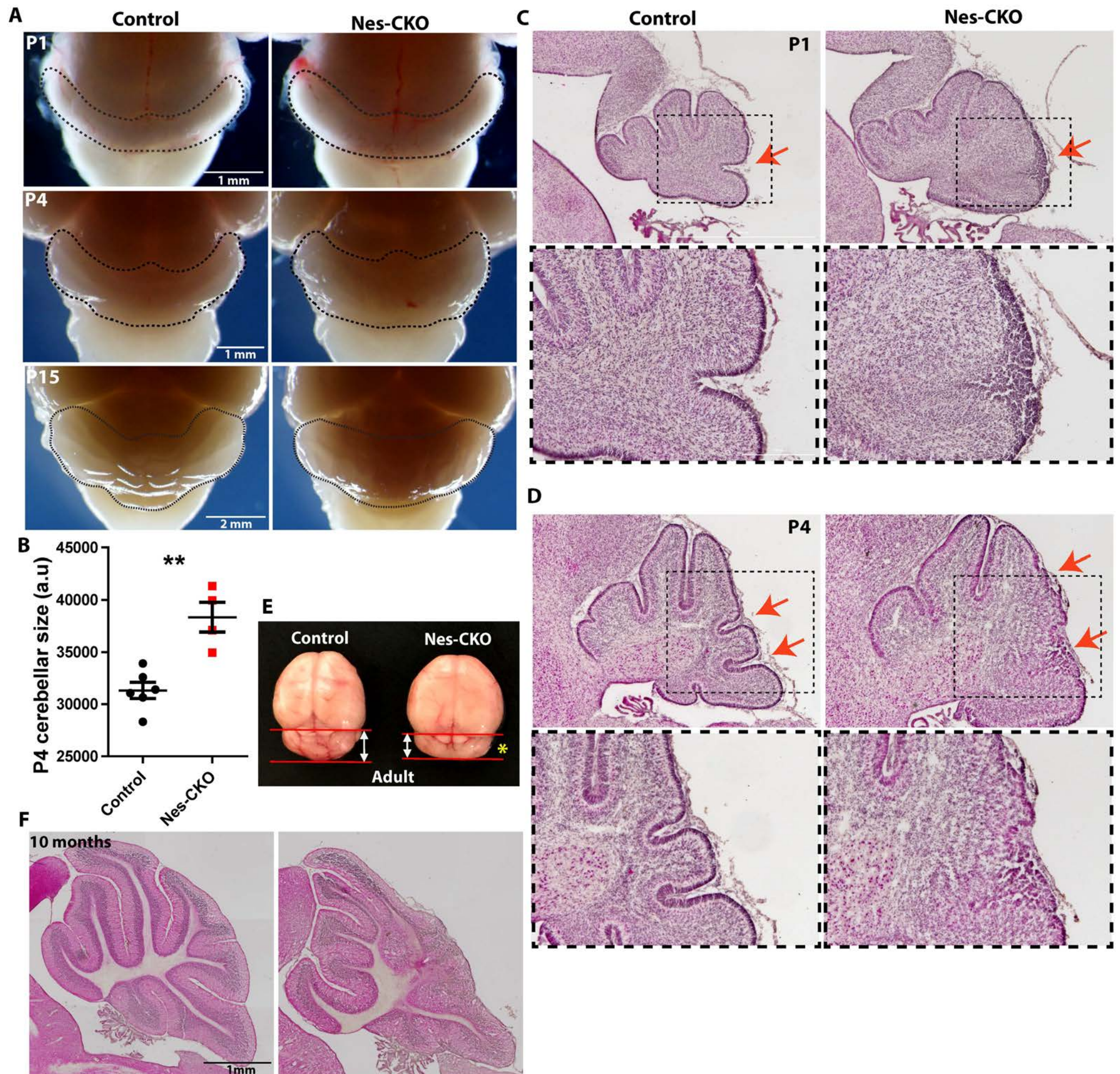


Figure 2

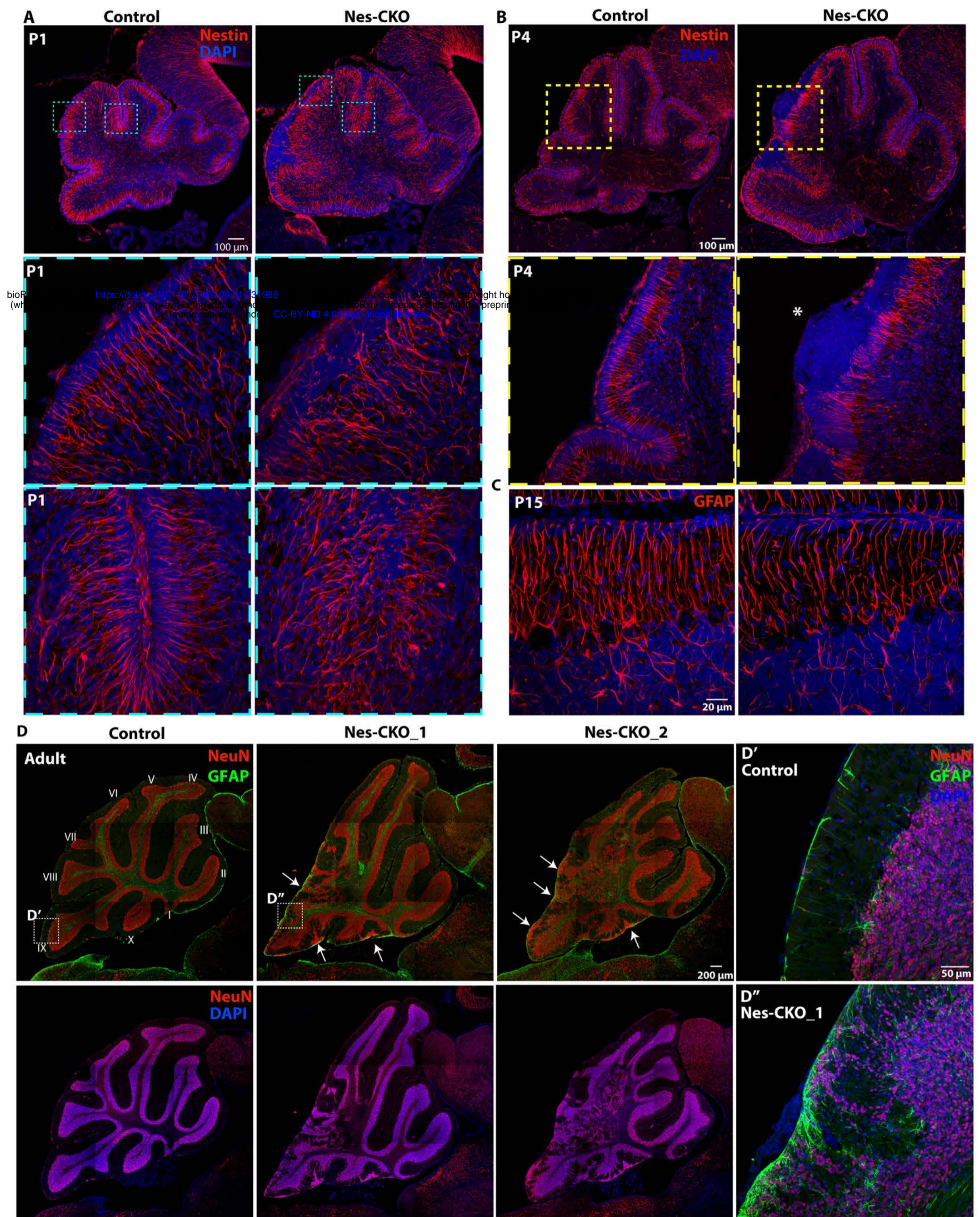


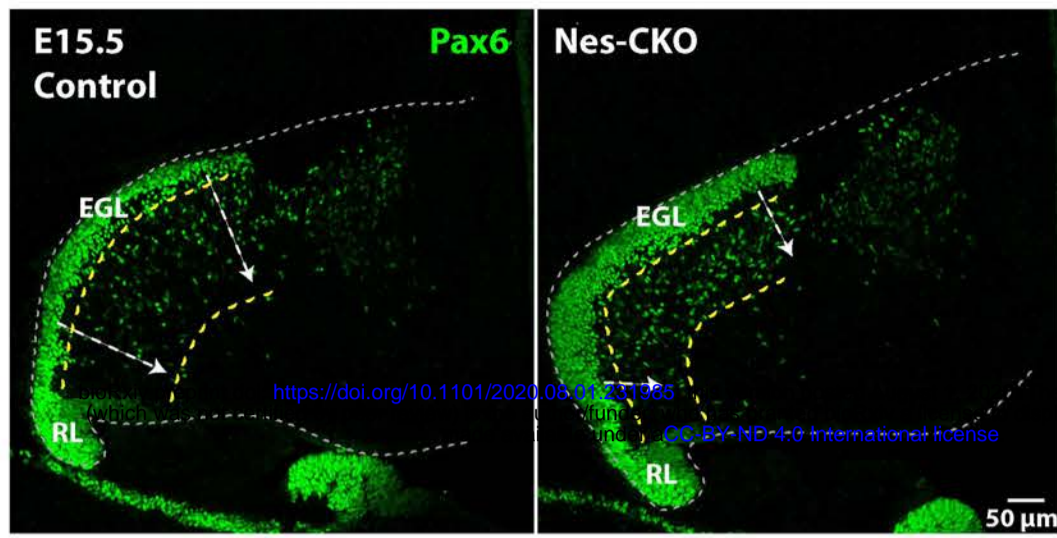
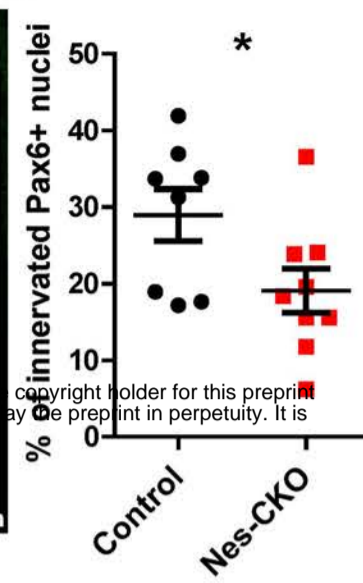
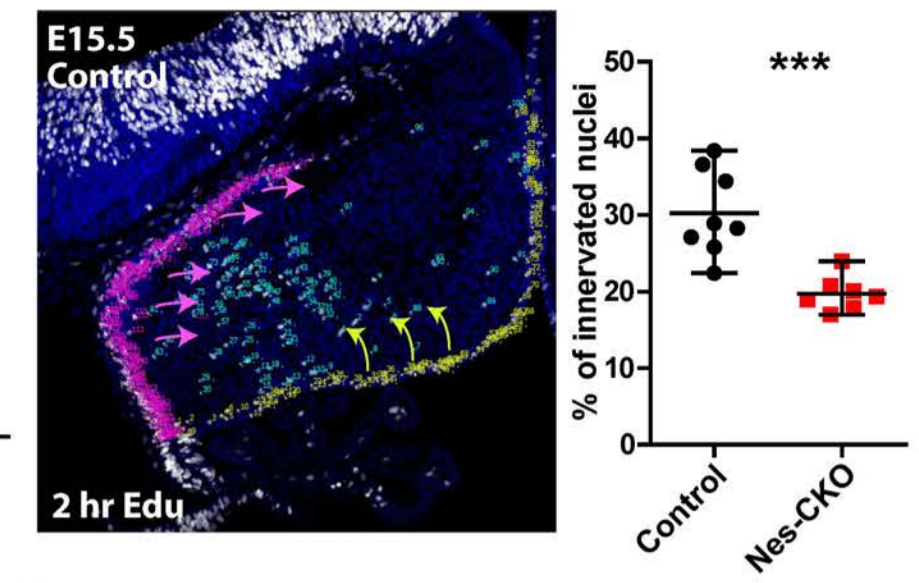
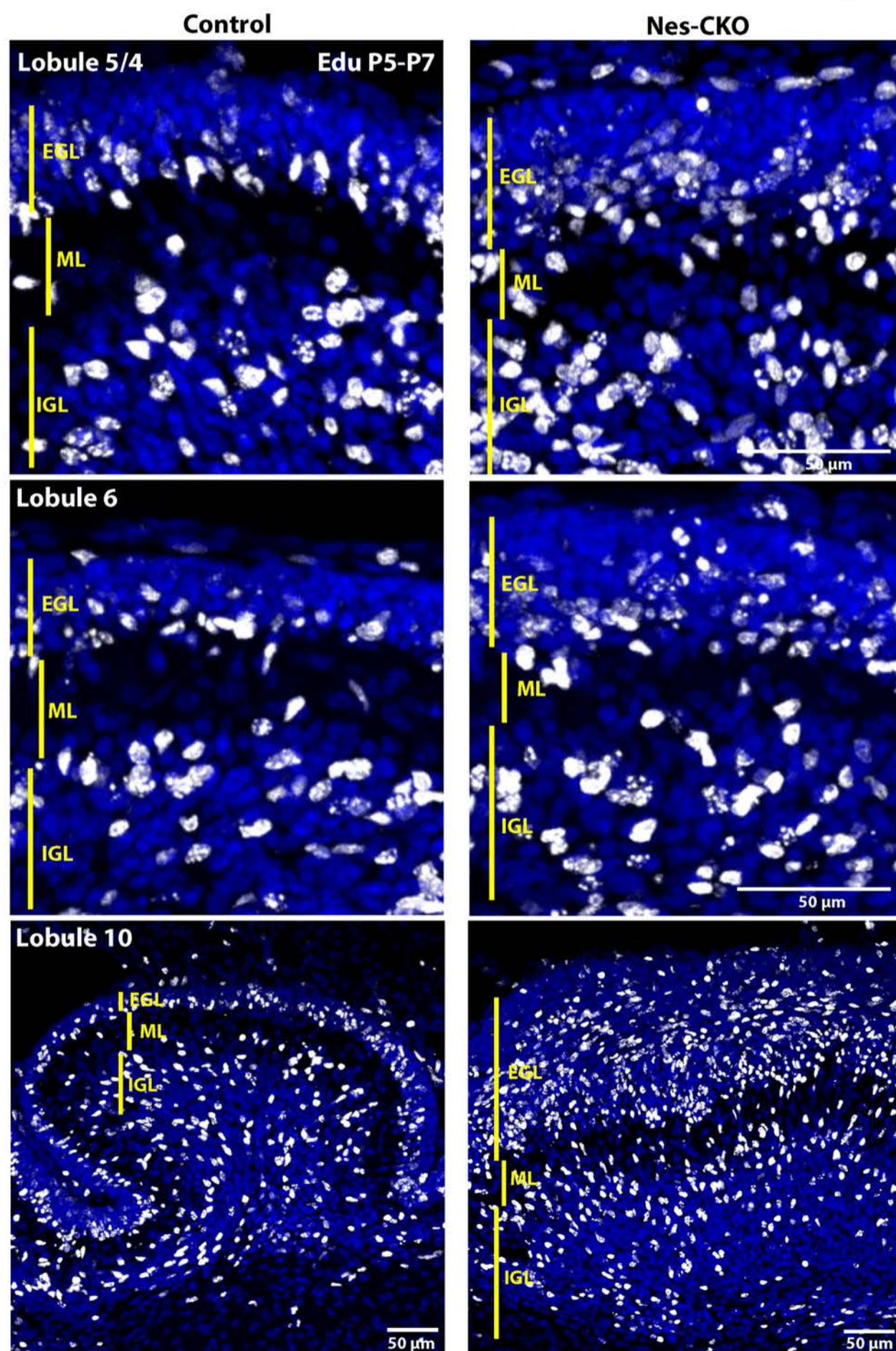
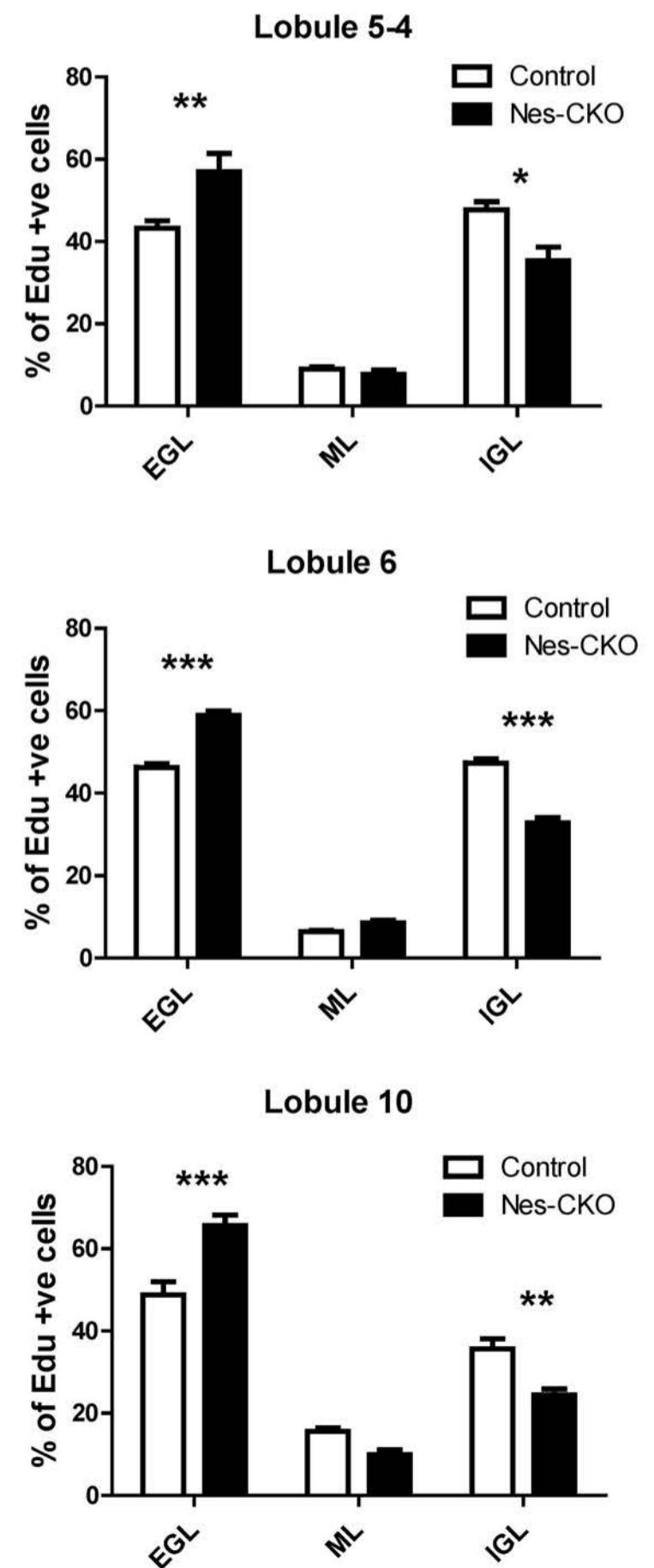
Figure 3**A****B****C****D****E**

Figure 4

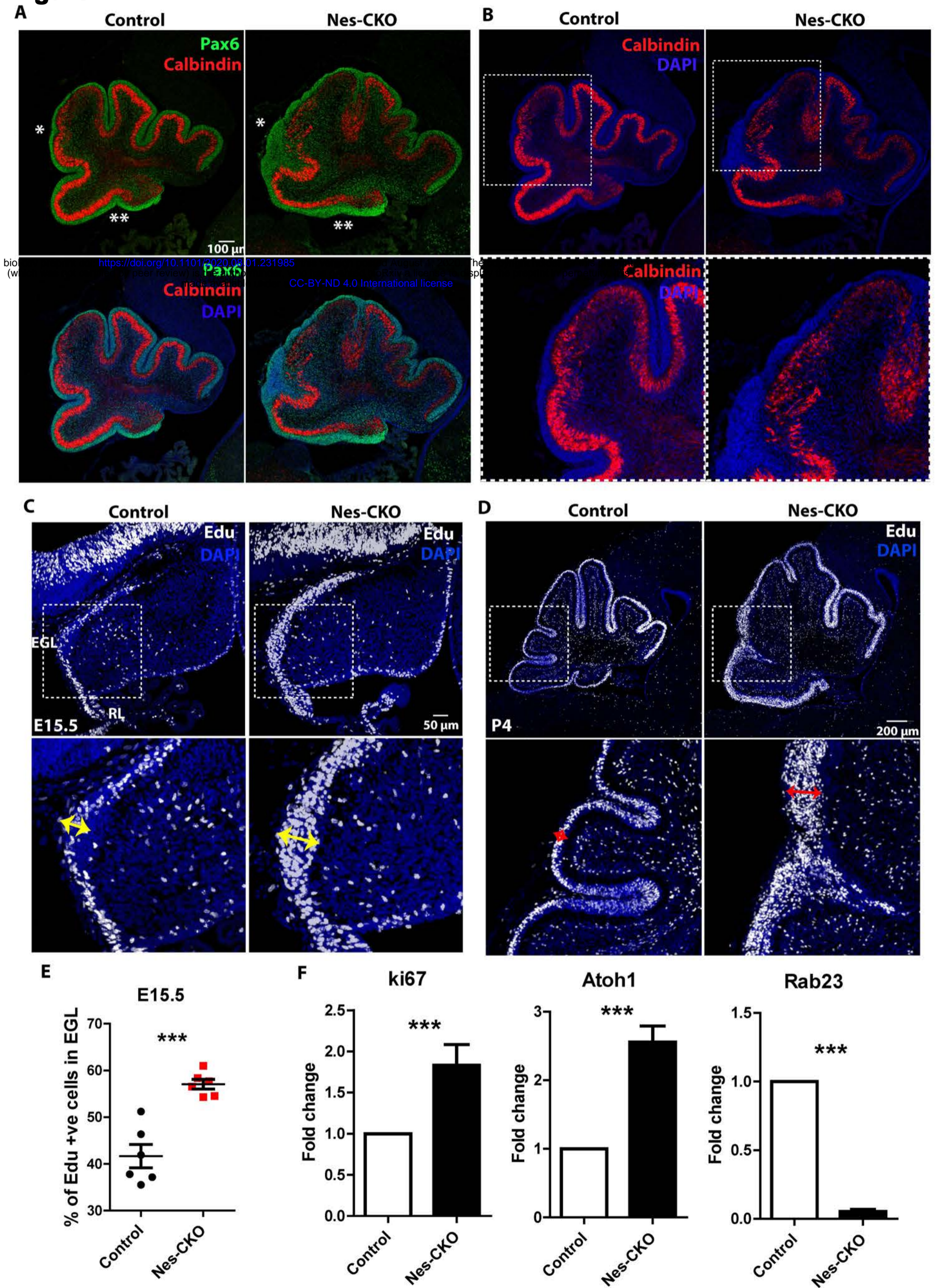
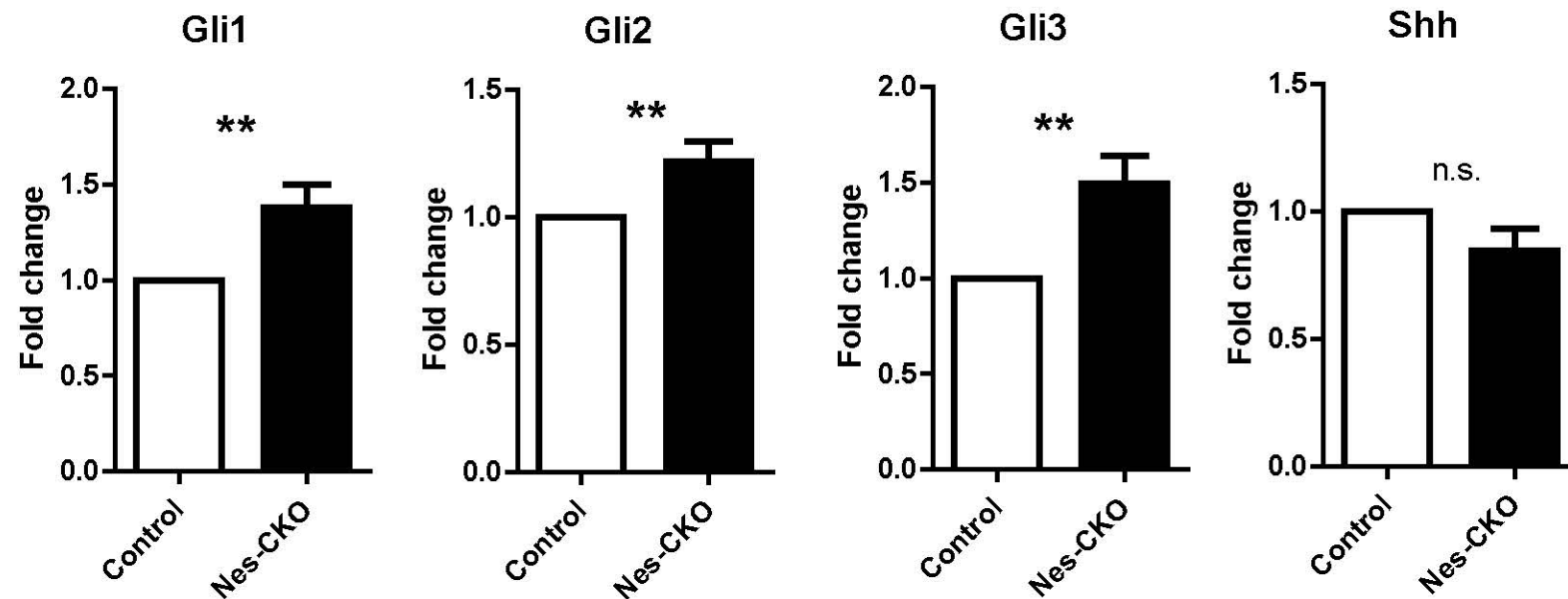


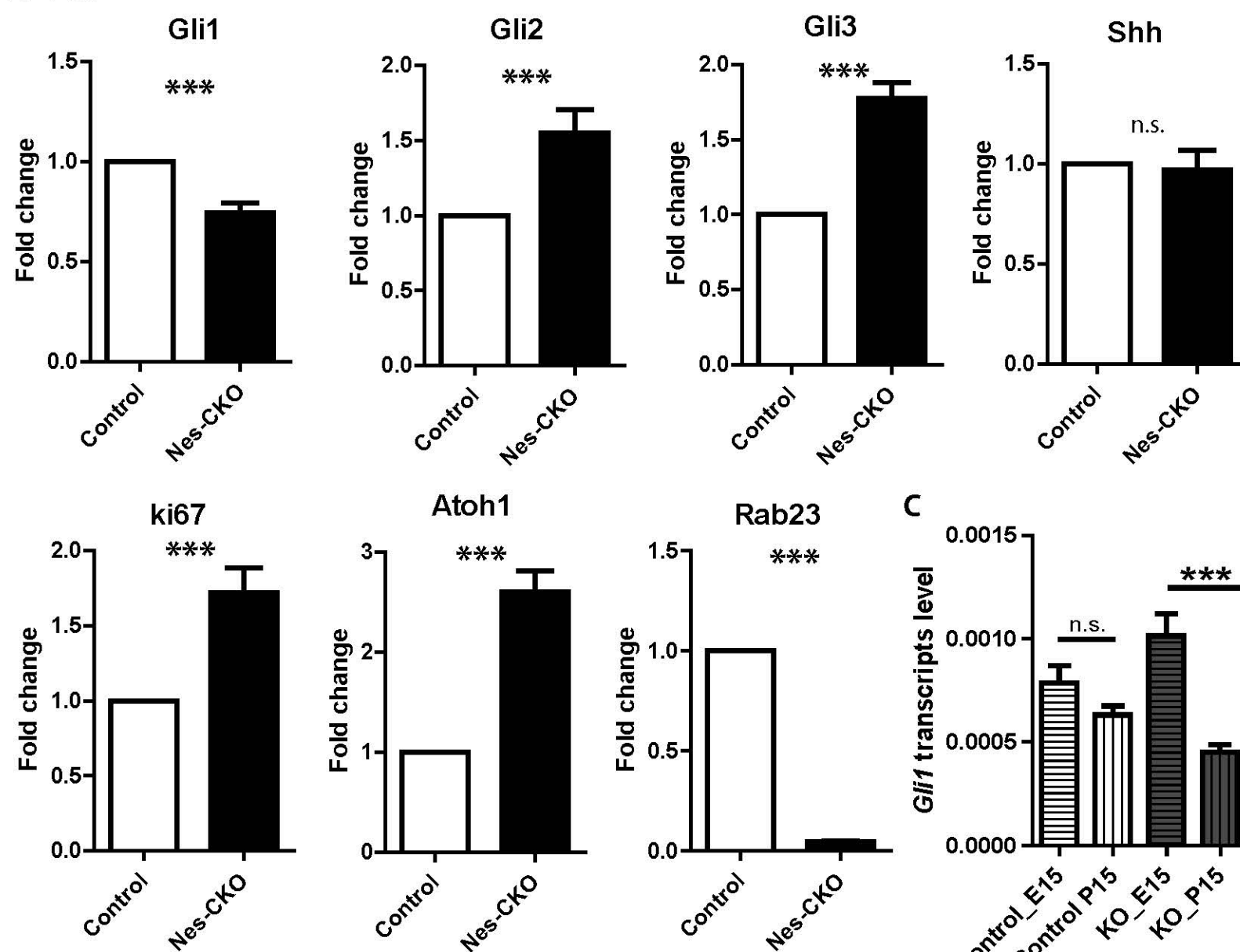
Figure 5

bioRxiv preprint doi: <https://doi.org/10.1101/2020.08.01.231985>; this version posted August 1, 2020. The copyright holder for this preprint (which was not certified by peer review) is the author/funder, who has granted bioRxiv a license to display the preprint in perpetuity. It is made available under a [CC-BY-ND 4.0 International license](https://creativecommons.org/licenses/by-nd/4.0/).

A E15.5



B P15



C

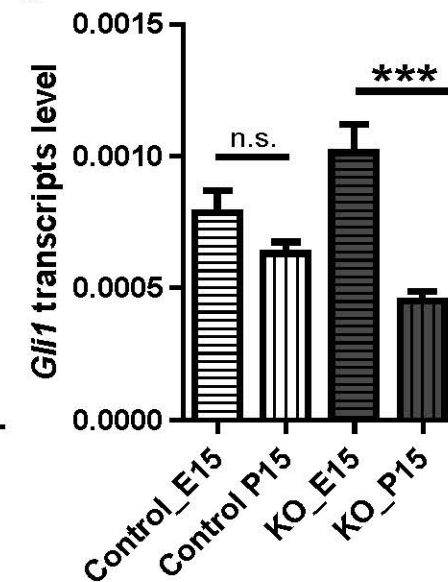


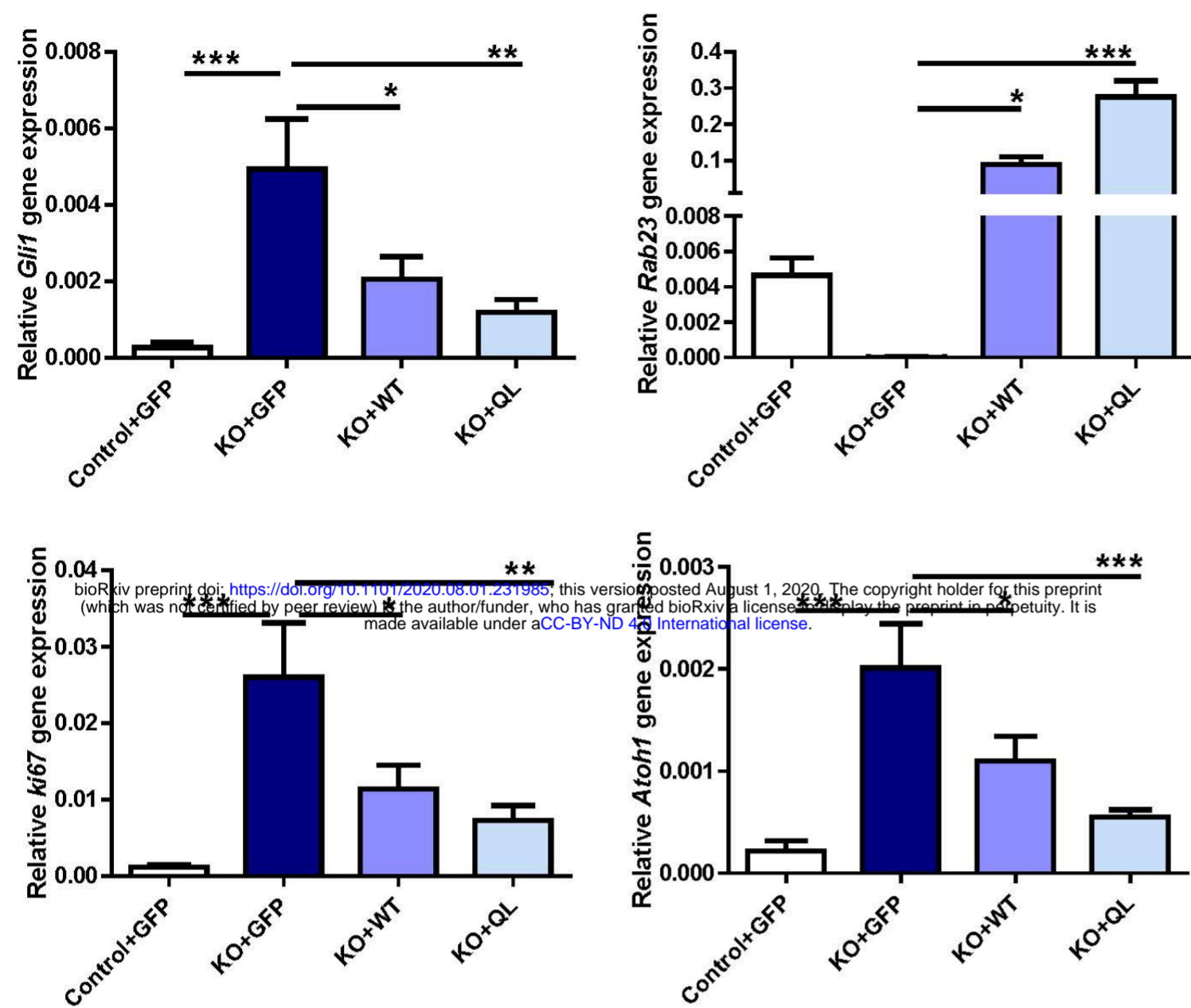
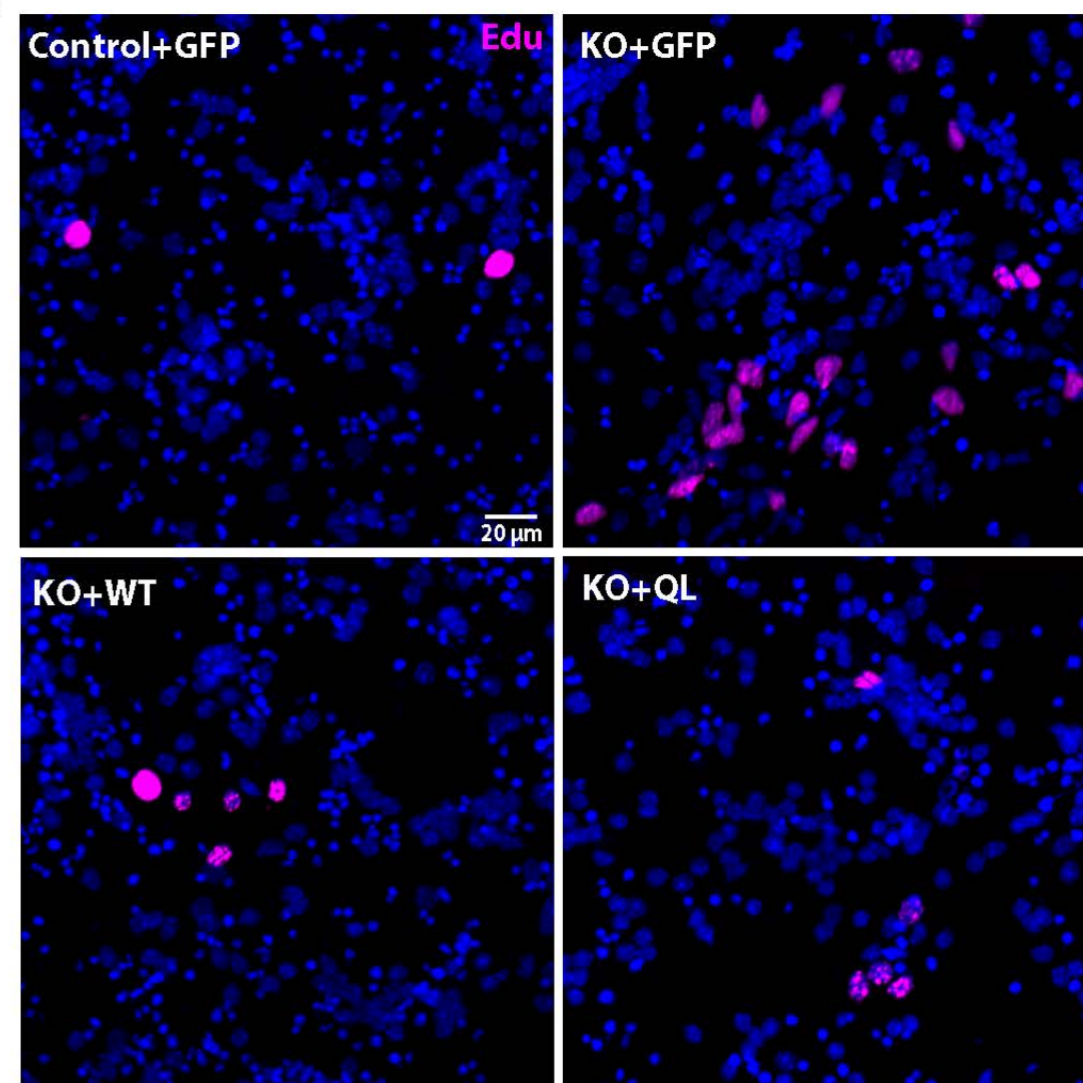
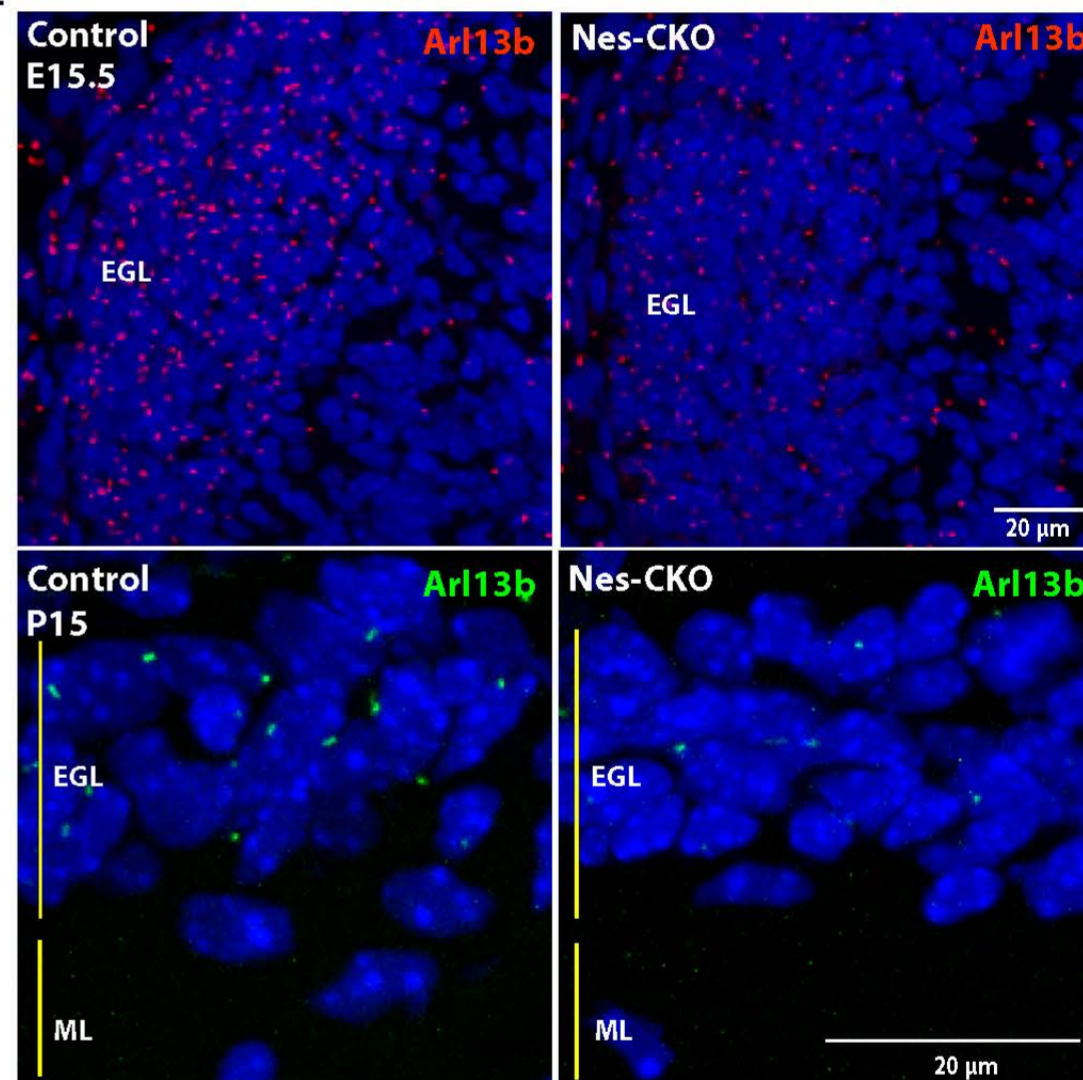
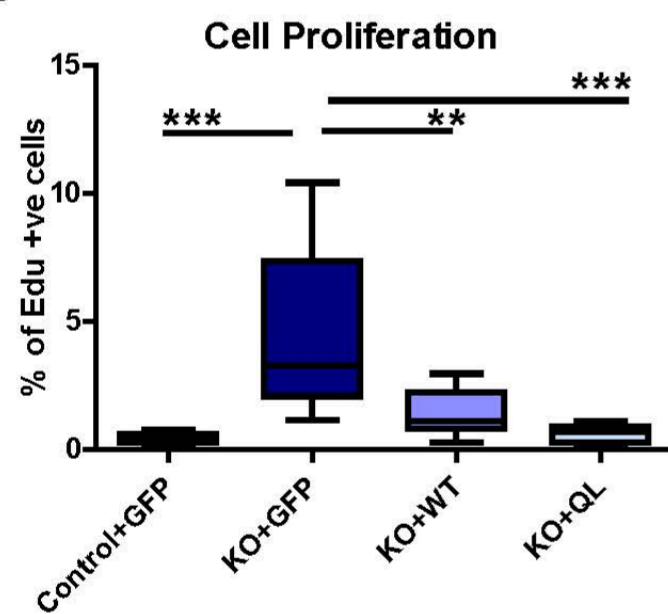
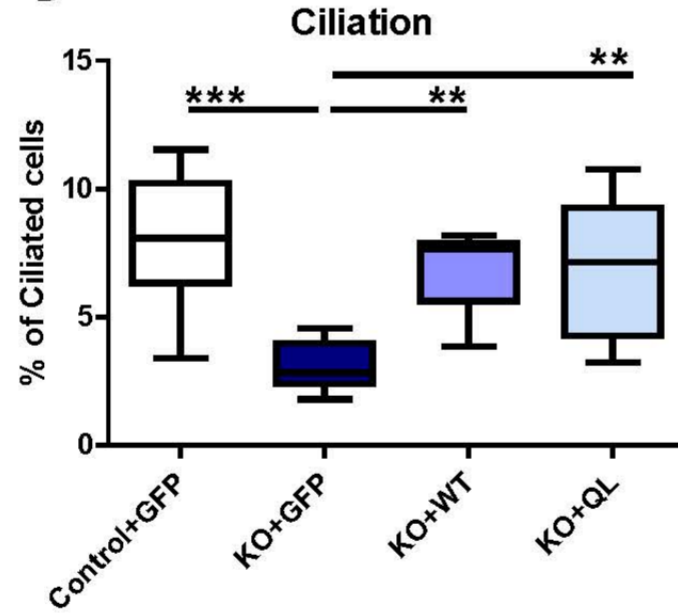
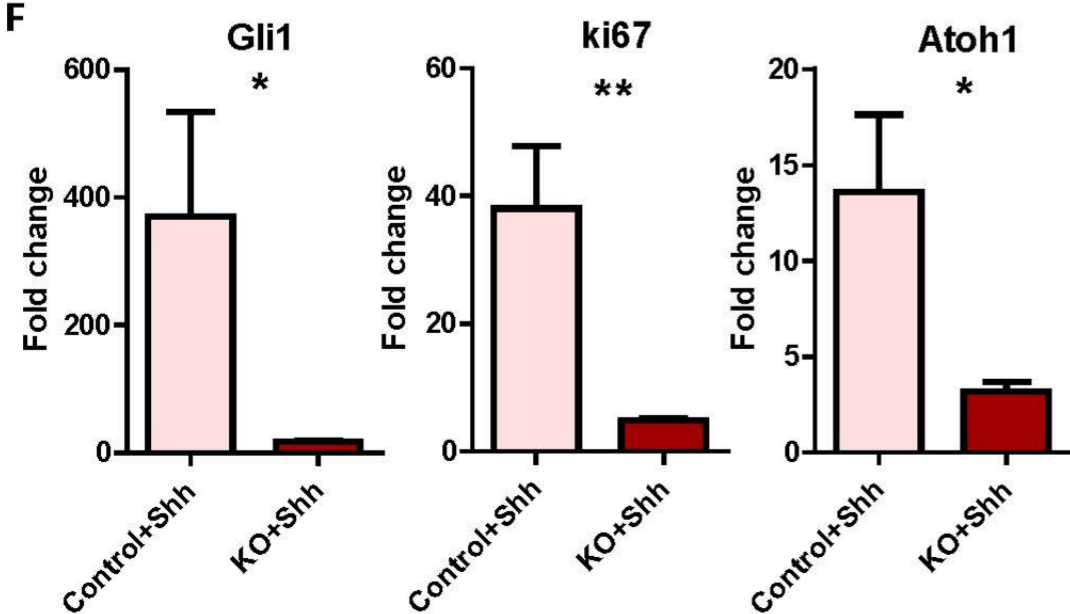
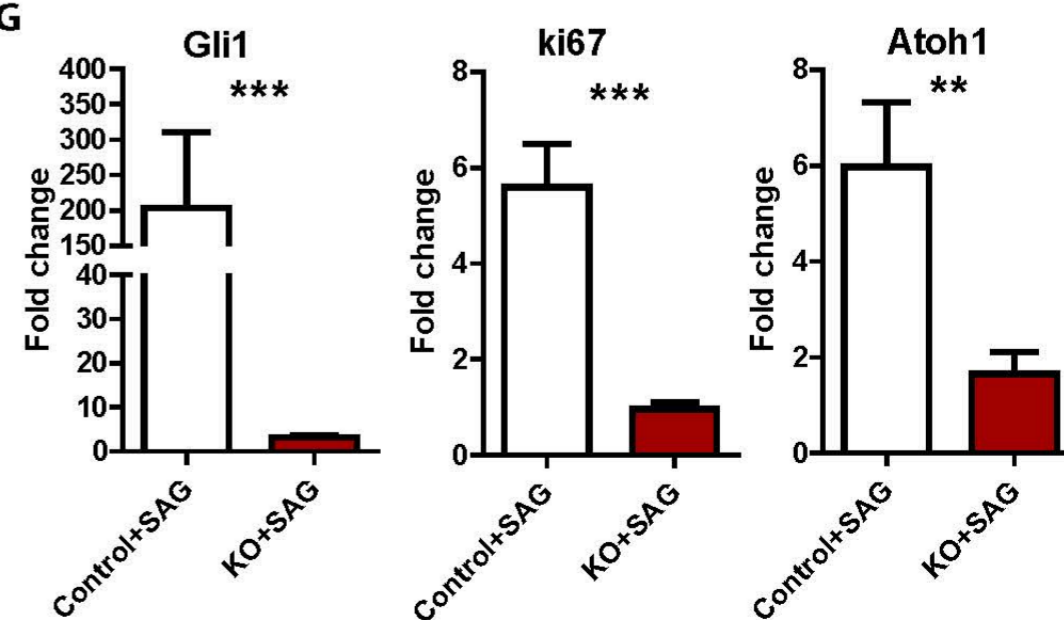
Figure 6**A****B****E****C****D****F****G**

Figure 7

